© 2017. Published by The Company of Biologists Ltd | Development (2017) 144, 464-478 doi:10.1242/dev.133926

RESEARCH ARTICLE

An exclusive cellular and molecular network governs intestinal smooth muscle cell differentiation in vertebrates

Dafne Gays[1], Christopher Hess[3], Annalisa Camporeale[1], Ugo Ala[1], Paolo Provero[1], Christian Mosimann[3] and Massimo M. Santoro[1,2,*]

ABSTRACT

Intestinal smooth muscle cells (iSMCs) are a crucial component of the adult gastrointestinal tract and support intestinal differentiation, peristalsis and epithelial homeostasis during development. Despite these crucial roles, the origin of iSMCs and the mechanisms responsible for their differentiation and function remain largely unknown in vertebrates. Here, we demonstrate that iSMCs arise from the lateral plate mesoderm (LPM) in a stepwise process. Combining pharmacological and genetic approaches, we show that TGFβ/*Alk5* signaling drives the LPM ventral migration and commitment to an iSMC fate. The Alk5-dependent induction of *zeb1a* and *foxo1a* is required for this morphogenetic process: *zeb1a* is responsible for driving LPM migration around the gut, whereas *foxo1a* regulates LPM predisposition to iSMC differentiation. We further show that TGFβ, *zeb1a* and *foxo1a* are tightly linked together by *miR-145*. In iSMC-committed cells, TGFβ induces the expression of *miR-145*, which in turn is able to downregulate *zeb1a* and *foxo1a*. The absence of *miR-145* results in only a slight reduction in the number of iSMCs, which still express mesenchymal genes but fail to contract. Together, our data uncover a cascade of molecular events that govern distinct morphogenetic steps during the emergence and differentiation of vertebrate iSMCs.

KEY WORDS: Zebrafish, Organogenesis, Lateral plate mesoderm, Smooth muscle cells

INTRODUCTION

Smooth muscle cells (SMCs) constitute a vital proportion of various organs, including those of the gastrointestinal (GI) tract, urogenital tract, respiratory tract and vascular system. Despite their crucial contribution to organ function, little is known about the ontogeny and genetic developmental programs that drive SMC differentiation in vertebrates. A key challenge to studying the mechanisms of SMC development and differentiation arises from the complex origin of SMCs from seemingly multiple and sometime unknown cell types (Kumar and Owens, 2003). Current concepts describe most SMCs as arising from the condensation of surrounding, vaguely defined mesenchyme under the control of local environmental cues. In coordination with the different cell types present in the developing organs, mesenchyme initially forms early-synthetic SMCs that later develop into mature contractile SMCs (Gabella, 2002). A complex SMC lineage is the intestinal SMCs (iSMCs), which is found around the enteric endoderm-derived epithelium. iSMCs are indispensable for proper gut organogenesis as they contribute to vilification and provide the contractility necessary for intestine functionality (Shyer et al., 2013). Defects in their development are apparent in human congenital disorders such as visceral myopathy.

Lateral plate mesoderm (LPM) is a highly dynamic mesoderm field composed of bilateral stripes of cells appearing in post-gastrula embryos. The LPM is patterned early into distinct regions that will give rise to precursors of kidney, heart, endothelium, hematopoietic and limb cell fates (Davidson and Zon, 2004; Gering et al., 2003; Mosimann et al., 2015). Although previous work has suggested that iSMCs arise from the lateral plate mesoderm (LPM), genetic demonstration for this origin is still missing in a vertebrate model (Roberts et al., 1998). Currently lacking is a cellular and molecular concept of how the bilateral precursor stripes form the smooth muscle layer surrounding the endoderm-derived gut tube, and whether these cells indeed derive from the LPM. How the possibly LPM-derived iSMC precursors induce and regulate their migration to converge on and surround the gut tube also remains unknown. In the past, early events of LPM and gut morphogenesis have been well described, taking advantage of the zebrafish model system (Horne-Badovinac et al., 2003; Stainier, 2005). The anatomical conservation and relative simplicity of its intestine have made the zebrafish an ideal vertebrate model for studying early gut development and endodermal differentiation (Bagnat et al., 2007; Horne-Badovinac et al., 2003; Wallace et al., 2005; Yin et al., 2010), and the initial characterization of iSMCs (Georgijevic et al., 2007; Wallace et al., 2005; Whitesell et al., 2014).

Organogenesis requires a highly coordinated series of molecular and cellular events. Among the different categories of molecules involved in organ formation and cell fate control, miRNAs represent a sophisticated level of gene regulation that coordinates a broad spectrum of biological processes, from development to cancer (Kloosterman and Plasterk, 2006). miRNAs are endogenous ∼22-nucleotide RNAs that control protein expression through translational repression of mRNAs. In cooperation with transcription factors, miRNAs can establish autoregulatory feedback loops and feed-forward loops, reaching high levels of complexity in the regulation of gene expression and subsequently of biological processes (Tsang et al., 2007).

Here, combining genetic, pharmacological and bioinformatics approaches, we characterize cellular and molecular events occurring during LPM differentiation and intestinal SMC development in zebrafish. Using genetic lineage tracing, we demonstrate that iSMCs arise from the LPM in a stepwise process. We show that a TGFβ- and Zeb1a-mediated migration of *hand2*-positive LPM cells around the gut endoderm drives commitment of epithelial LPM into mesenchymal iSMC progenitors. TGFβ/Alk5 signaling also leads to the expression of *miR-145* that is required to switch off the

[1]Department of Molecular Biotechnology and Health Sciences, Molecular Biotechnology Center, University of Torino, Turin 10126, Italy. [2]Vesalius Research Center, VIB-KUL, Leuven 3000, Belgium. [3]Institute of Molecular Life Sciences (IMLS), University of Zürich, Zürich 8057, Switzerland.

*Author for correspondence (massimo.santoro@unito.it)

M.M.S., 0000-0003-4605-5085

Received 8 December 2015; Accepted 9 December 2016

Development (2017) 144, 464-478 doi:10.1242/dev.133926

migrating signature of the LPM and to downregulate translation of the Forkhead transcription factor gene *foxo1a*, a novel component of LPM and iSMC differentiation. Together, our data uncover a sequence of unique molecular events that govern distinct steps during the emergence and differentiation of iSMCs from migrating LPM in vertebrates. Understanding of how iSMCs develop is key to targeting smooth muscle cell-related pathologies and to improve prognostic and therapeutic approaches.

RESULTS

Lateral plate mesoderm gives rise to intestinal SMCs

Previous reports indicated that zebrafish embryos mutant for the LPM-expressed transcription factor gene *hand2* (heart and neural crest derivatives expressed 2) (Yelon et al., 2000) completely lack iSMCs (Santoro et al., 2009). To investigate how LPM emergence and differentiation are related to iSMC formation, we combined different approaches.

We first tracked LPM derivatives in a BAC-based reporter transgenic line *Tg(hand2:EGFP)*^{pd24} based on the endogenous *hand2 cis*-regulatory elements that also express in the presumptive posterior LPM from early somitogenesis onwards [*Tg(hand2:EGFP)*^{pd24}] (Yin et al., 2010). Using confocal microscopy of transverse embryo cross-sections, we examined EGFP expression between somites 7 and 13, a region in which the enteric endoderm is located at the midline (i.e. above the yolk extension; Fig. 1A and Fig. S1A). By 24 h post-fertilization (hpf), *hand2*-expressing cells in zebrafish embryos form bilateral mesodermal sheets spanning the entire anterior-posterior (A-P) extent of the trunk. At this time point, this remaining undifferentiated LPM is located lateral to the gut and is composed of polarized proliferating epithelial cells (Horne-Badovinac et al., 2003; Yin et al., 2010). By 30 hpf, these *hand2*-expressing epithelial sheets started to cover the dorsal region of the gut endoderm. By 36 hpf, the LPM had enfolded the region underneath the endoderm through a process reminiscent of mesenchymalization. By 48 hpf, the gut tube was completely surrounded by *hand2*-expressing cells. From 60 hpf onwards, these *hand2*-positive cells expressed *acta2* (α-smooth muscle actin) and *tagln* (transgelin or *sm22a-b*). These genes are the earliest known markers of committed smooth muscle progenitor cells in vertebrates and remain expressed in differentiated SMCs (Georgijevic et al., 2007; Solway et al., 1995; Santoro et al., 2009). By 96 hpf, iSMCs were fully differentiated in contractile longitudinal and circular smooth muscle fibers, and promoted peristaltic movement of the gut in preparation for the onset of exogenous feeding (Wallace et al., 2005).

To further characterize the morphogenesis of the *hand2*-expressing LPM, we tested expression of epithelial markers, such as aPKC (atypical protein kinase C), and markers of mesenchymalization, such as N-cadherin, in the LPM from 24 hpf onwards (Fig. 1B,C). These results revealed that *hand2*-expressing bilateral LPM cells express both markers of epithelial and mesenchymal cells as early as 24 hpf. Our data support the possibility that the LPM cells acquire the feature of a collective migrating epithelial mesenchyme, a common event during embryonic developmental and tissue repair (Rørth, 2012).

By 72 hpf, a subpopulation of *hand2*-expressing LPM cells start to express the SMC marker Tagln. As shown in Fig. 1C, all the Tagln-positive cells are also positive for *hand2* expression, supporting the conclusion that all the iSMCs originate from LPM/*hand2*+ cells (Fig. 1D). *Tg(hand2:EGFP)*^{pd24} also exhibited EGFP-positive cells located in the enteric submucosa that were negative for Tagln but positive for Hu, a marker specific for neurons (Fig. S1B). As *hand2* is also expressed in neural crest derivatives and is required for the development of neural crest-derived neurons (Olden et al., 2008; Reichenbach et al., 2008), we concluded these cells are enteric neurons. Taken together, our observations confirm and extend previous reports that *hand2*-expressing bilateral LPM cells give rise to the iSMC layer surrounding the developing gut tube.

As a second and independent approach to link iSMCs to an LPM origin, we performed Cre/*lox*-mediated lineage tracing in the *Tg(drl:creERT2)* line, which uniquely expresses tamoxifen-inducible Cre recombinase in all presumptive LPM precursors already during late epiboly (Mosimann et al., 2015). We crossed *drl:creERT2* with the ubiquitous GFP-to-mCherry *loxP* lineage trace transgene *ubi:Switch* (Mosimann and Zon, 2011) and induced Cre activity at late epiboly/tailbud stages, when *drl* transgene expression is confined to presumptive LPM cells. We detected lineage-labeled precursor iSMCs at 72 hpf and iSMCs around the gut along the entire length of the trunk, concomitant with the expected LPM-derived lineage labeling of the pronephric duct and endothelial cells (Fig. 2A). Lineage-labeled cells surrounding the gut co-stained with the iSMC marker Tagln as early as 72 hpf (Fig. 2B and Fig. S2B). We found lineage-labeled iSMCs in all embryos treated with 4-OH at 1 ss (n=31) (Fig. 2C). In all embryos tested, we observed different grades of switching efficiency, ranging from a few iSMC labeled (class I) cells to complete lineage labeling of all gut-surrounding iSMCs (class III). The variability and efficiency corresponds to the ubiquitous *ubi:Switch* recombination capacity in controls (Fig. S2A) and in our previous *ubi:Switch* characterizations (Felker et al., 2016). Taken together, our genetic lineage tracing results demonstrate that initially *drl*-expressing and subsequently *hand2*-expressing LPM cells form mesenchymal cells that later on become iSMCs. Altogether, our data show that the LPM gives rise to iSMCs in zebrafish and support the notion that the signaling and genetic pathways driving the emergence and differentiation of the LPM might also underlie iSMC formation.

LPM requires TGFβ signaling to differentiate into iSMCs

To specifically track the development and maturation of iSMCs, we next derived two independent transgenic zebrafish reporter lines with fluorescent markers under the control of the *acta2* and *tagln* minimal *cis*-regulatory elements (Fig. S3A,B; see Materials and Methods for details). Although reporter expression in these lines differed in intensity and specificity, both *Tg(acta2:mCherry)*^{uto5} and *Tg(tagln:CAAX-EGFP)*^{uto37} embryos exhibit fluorescent marker expression in immature iSMCs beginning at 60-72 hpf. By 96 hpf and through adulthood, both reporter lines mark mature and contractile iSMCs covering the entire intestine and swim bladder (Fig. S3A,B). Our new *acta2* and *tagln* transgenic reporters are therefore bona fide reporter lines for immature and mature iSMCs.

We next used our *acta2* and *tagln* reporter lines as readouts to screen for signaling pathways that drive iSMC formation using a panel of established chemical inhibitors (Table S2). Chemical inhibition from 20 hpf of the TGFβ type I receptors by SB431542 and LY364947 selectively impaired iSMC development (Fig. 3A,B and data not shown). We further confirmed the role of TGFβ in iSMCs by analyzing *ltbp3* morphants that were previously shown to specifically phenocopy Alk5 inhibition (Zhou et al., 2011). Both pharmacological and genetic perturbation of TGFβ signaling disrupted iSMC differentiation *in vivo* without interfering with overall gut endoderm specification and morphology (Fig. 3A,B and Fig. S3C). To confirm these data, we then evaluated iSMCs differentiation markers in *Tg(hsp70:caALK5)*, in which heat shock triggers constitutive Alk5 activity and signaling (Zhou et al., 2011).

Development (2017) 144, 464-478 doi:10.1242/dev.133926

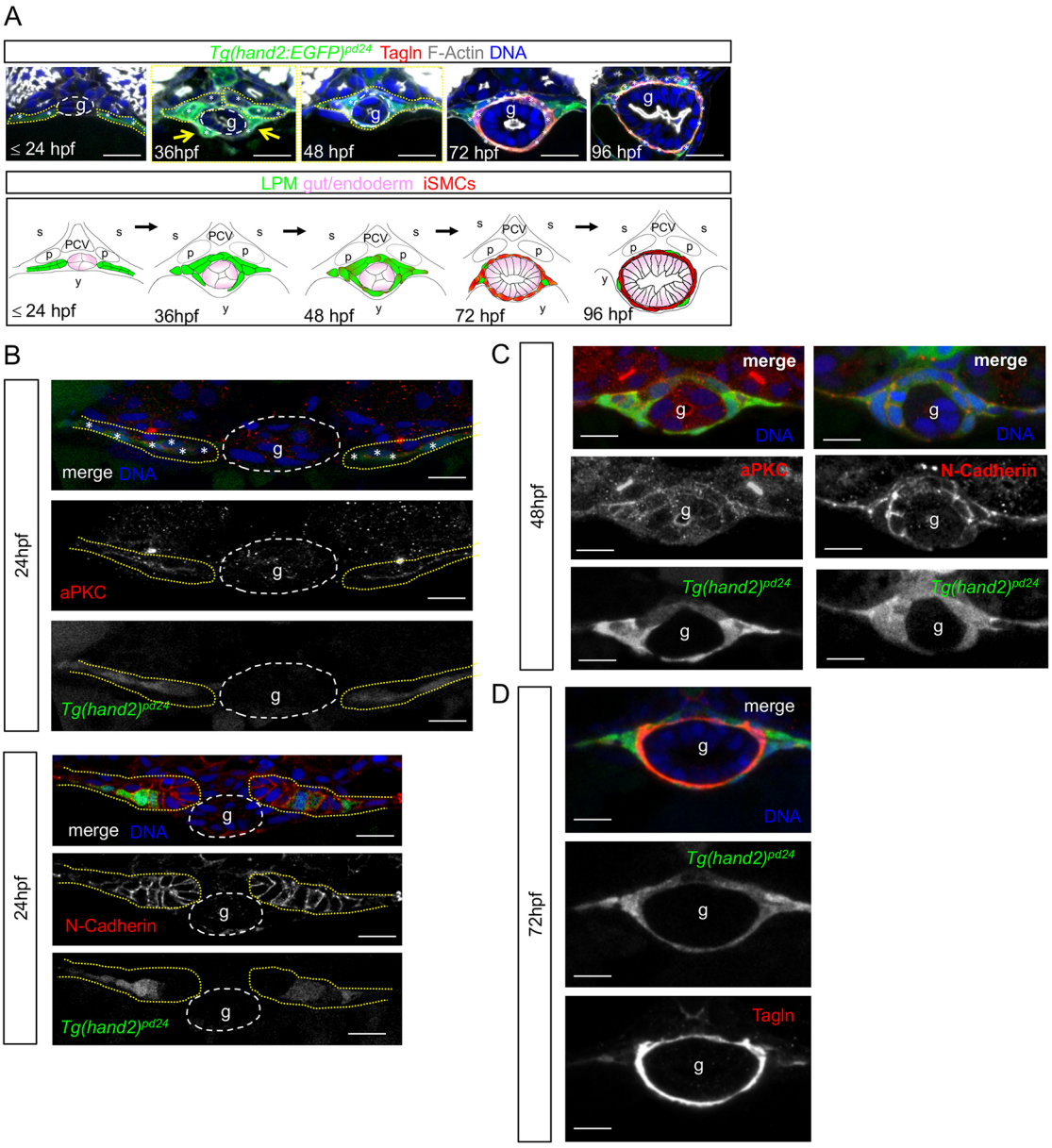

Fig. 1. LPM gives rise to iSMCs in zebrafish embryos. (A) Time-course analyses of *Tg(hand2:EGFP)*^{pd24} and iSMC marker expression (Tagln) during intestinal development. *Tg(hand2:EGFP)*^{pd24} embryos were fixed at different time points from 24 hpf until 96 hpf. Upper panel: confocal transverse sections of the posterior gut region between the somites 7 and 13 of *Tg(hand2:EGFP)*^{pd24} embryos stained with phalloidin (gray) and Tagln (red) (single channels are shown in Fig. S1A). The dashed yellow lines highlight LPM/*hand2*+ cells, whereas the dashed white lines highlight the enteric endoderm (g). Migration of the LPM is indicated by arrows. Asterisks indicate single-cell nuclei. ISMC differentiation is visible during intestinal development by expression of Tagln; blue indicates nuclei; g, gut. Scale bar: 30 µm. Bottom panel: schematic representation of LPM/*hand2*+ conversion to iSMCs in the gut region of developing zebrafish embryos. Green, LPM; pink, endoderm; red, iSMCs; p, pronephros; s, somite; PCV, posterior cardinal vein; y, yolk. (B) Analyses of *Tg(hand2:EGFP)*^{pd24} and polarity and mesenchymal markers during LPM development at 24 hpf. Confocal transverse sections of the posterior gut region between the somites 7 and 13 of *Tg(hand2:EGFP)*^{pd24} embryos stained with aPKC or N-cadherin. Nuclei are in blue; g, gut. Scale bars: 30 µm. Asterisks indicate single-cell nuclei while the dashed yellow lines highlight LPM/*hand2*+ cells. (C) Analyses of *Tg(hand2:EGFP)*^{pd24} and polarity and mesenchymal markers during LPM development at 48 hpf. Confocal transverse sections of the posterior gut region between the somites 7 and 13 of *Tg(hand2:EGFP)*^{pd24} embryos stained with aPKC (left, red) or N-cadherin (right, red). Blue indicates nuclei; g, gut. Scale bars: 30 µm. (D) Analyses of *Tg(hand2:EGFP)*^{pd24} and iSMC marker expression (Tagln) at 72 hpf. Confocal transverse sections of the posterior gut region between the somites 7 and 13 of *Tg(hand2:EGFP)*^{pd24} embryos stained with Tagln (red) show that all differentiated iSMC are also *Tg(hand2:EGFP)*^{pd24} positive. These observations suggest that posterior LPM expression of *hand2* does not demarcate the entire LPM, but rather is confined to the presumptive iSMC progenitors from its expression onset after LPM formation. Nuclei are in blue; g, gut. Scale bars: 30 µm.

Heat-shock-induced expression of constitutively active Alk5 increased *acta2*, *tagln* and *myh11* expression, further supporting the role of TGFβ signaling in promoting iSMC mainly through Alk5 receptor (Fig. S3D).

One of the key functions of TGFβ signaling during development is to promote cell migration and invasion (Lim and Thiery, 2012; Zhang et al., 2014). We consequently hypothesized that TGFβ could also control the migration of

Development (2017) 144, 464-478 doi:10.1242/dev.133926

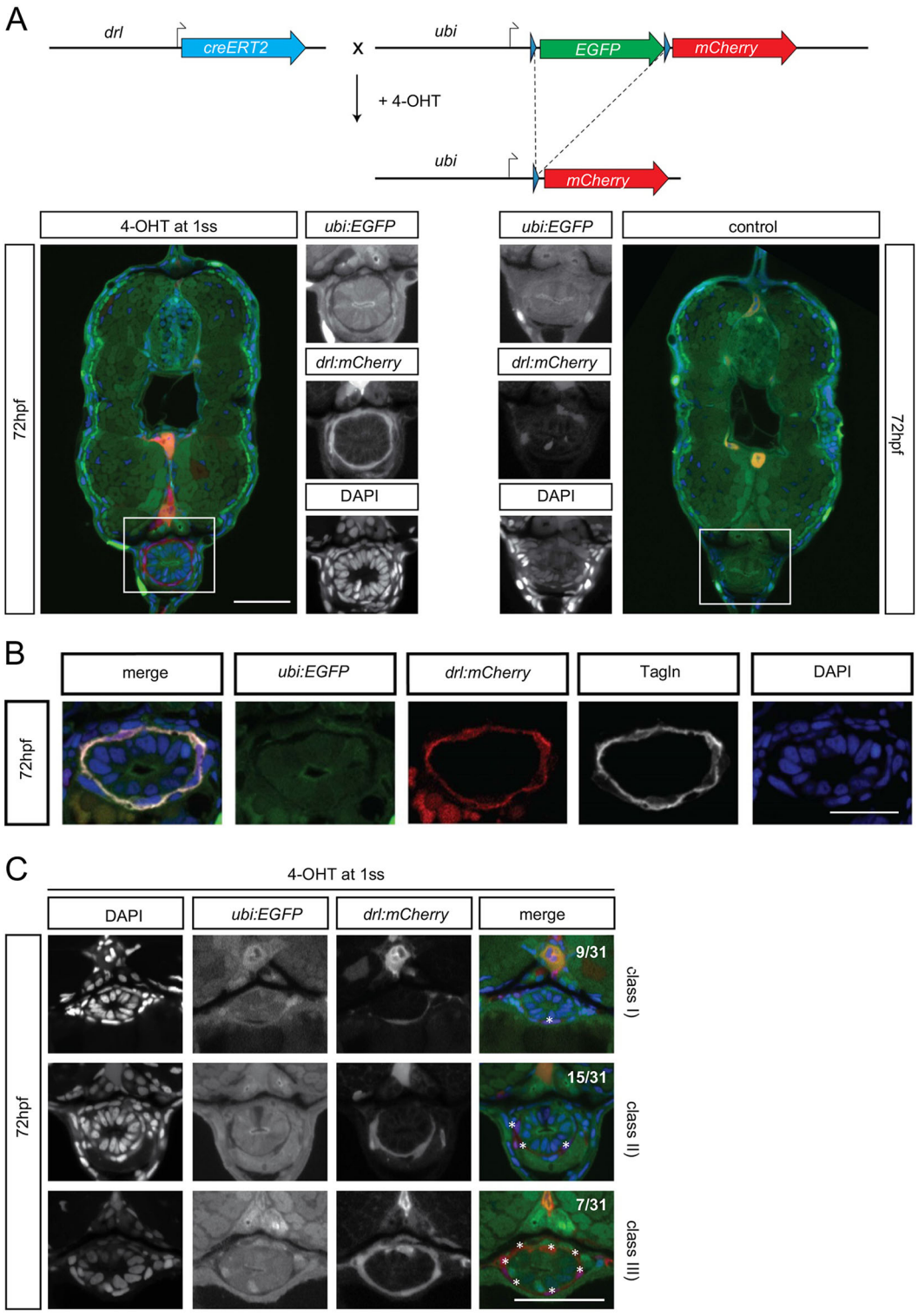

Fig. 2. *drl*-positive LPM cells give rise to iSMC. (A) Schematic of the *drl:creERT2*×*ubi:lox-EGFP-lox-mCherry* (*ubi:switch*) crosses. Double-positive embryos were induced at the one-somite stage with 4-OH tamoxifen (10 µM final concentration). This activates the Cre recombinase, which then excises the loxP-flanked *EGFP* cassette and brings *mCherry* under control of the *ubi* promoter to lineage trace the switched cells. Photomicrographs of transverse vibratome sections of posterior trunk region (*dr:creERT2;ubi:Switch*) are shown below. Sections were imaged with a Zeiss LSM710 40× objective. Scale bar: 50 µm. Higher magnification of the intestinal region. The merged channel comprises EGFP, mCherry and DAPI. (B) Transverse vibratome sections of the posterior trunk region (*dr:creERT2;ubi:Switch*). Higher magnifications of the intestinal region. iSMCs are stained using transgelin antibody to compare with lineage labeling by *drl:creERT2*. Scale bar: 30 µm. The merged channel comprises EGFP, mCherry and DAPI. (C) Transverse vibratome sections of the posterior trunk region (*drl:creERT2xubi:switch*). Higher magnification of the intestinal region showing the different switching efficacy for iSMCs after 4-OH treatment at the one-somite stage. Class I, few iSMC are switched; class II, half iSMC are switched; class III, the entire population of iSMCs surrounding the gut are switched. The occurrences of the switching efficacies are: class I, 28% (9/31); class II, 50% (15/31); class III, 22% (7/31). Asterisks indicate switched iSMCs. Sections were imaged with a Zeiss LSM710 40× objective. Scale bar: 25 µm. The merged channel comprises EGFP, mCherry and DAPI.

Development (2017) 144, 464-478 doi:10.1242/dev.133926

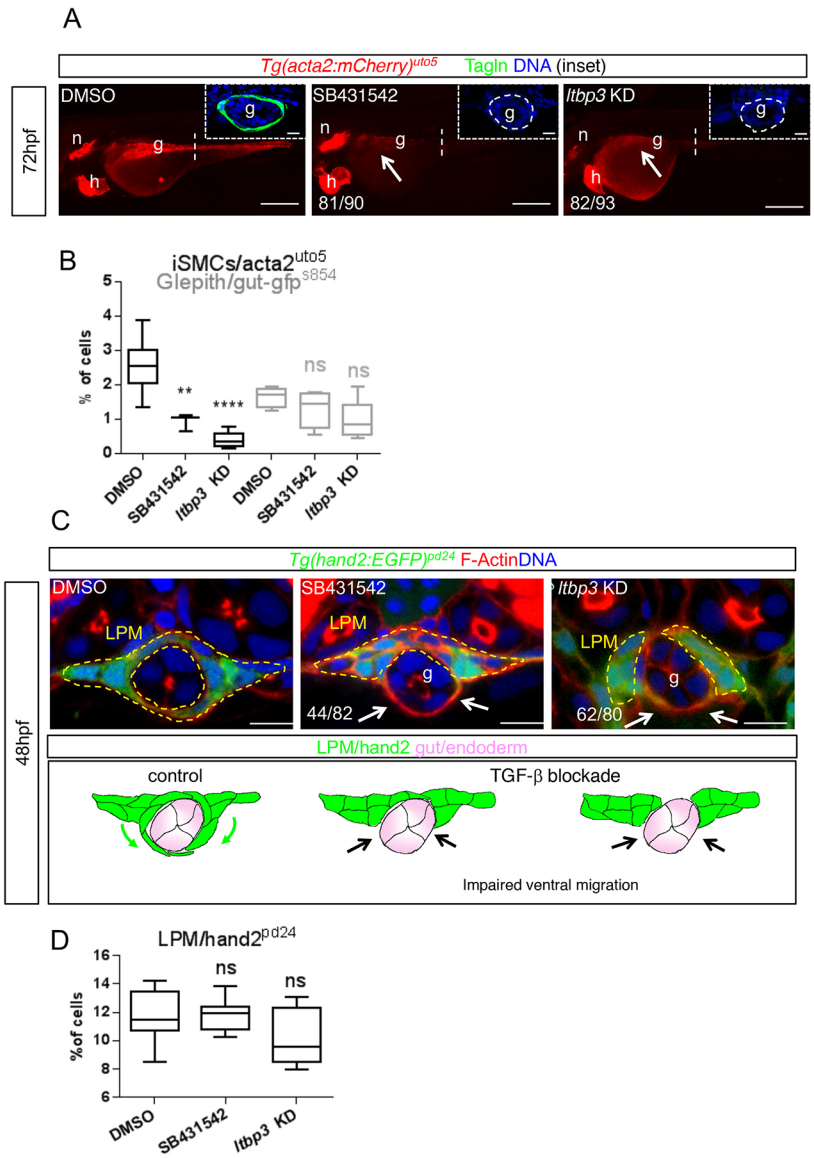

Fig. 3. LPM migration is guided by TGFβ signaling. (A) Pharmacological and genetic TGFβ signaling blockade impairs iSMC differentiation. Fluorescent images of *Tg(acta2:mCherry)*^{uto5} embryos treated with SB431542 (a TGFβ type I receptors inhibitor) or *ltbp3* knockdown (encoding a protein that regulates the bioavailability of TGFβ ligands) exhibit no or few iSMCs, as evaluated by mCherry and Tagln expression in the gut region (g) (arrow) at 72 hpf. Scale bars: 200 µm. n, notochord; h, heart. Insets show confocal transverse sections of posterior gut regions (dashed vertical line) of SB431542-treated embryos and embryos injected with *ltbp3* morpholino and stained for Tagln (green). The numbers of embryos showing the phenotype are indicated. Blue indicates nuclei. Scale bars in insets: 10 µm. (B) Alk5 blockade does not affect endoderm development and differentiation. Box and whisker plots show the percentage of iSMCs or endodermal cells isolated by fluorescent-activated cell sorting (FACS) experiments from the trunks spanning from somite 1 to 13 of the double *Tg(acta2:mCherry)*^{uto5} *(Xia.Eef1a1:GFP)*^{s854} embryos at 72 hpf after chemical (SB431542) or genetic (*ltbp3* KD) Alk5 signaling blockade. The boxplots show the maximum, minimum, upper and lower quartiles, and the sample median. Asterisks represent the results of one-way ANOVA-Dunnett's post-hoc test (**P<0.01, ****P<0.0001; from left to right: n=8, n=3, n=5, n=5, n=5 and n=5 groups of 10-20 embryos). (C) Blockade of TGFβ signaling impairs LPM migration. Upper panel: confocal transverse sections of *Tg(hand2:EGFP)*^{pd24} stained with phalloidin (red) and Hoechst (blue) showing a reduced LPM migration at 48 hpf (arrows) after TGFβ inhibition. Scale bars: 15 µm. The number of embryos exhibiting this phenotype is indicated. Lower panel: schematic representation of impaired LPM migration (black arrows) observed with the lack of TGFβ signaling in zebrafish embryos. Green, LPM; pink, endoderm. (D) Alk5 blockade does not affect LPM. Box and whisker plots show the percentage of LPM cells isolated by fluorescent-activated cell sorting (FACS) experiments from the trunks of *Tg(hand2:EGFP)*^{pd24} embryos at 48 hpf after chemical (SB431542) or genetic (*ltbp3* KD) Alk5 signaling inhibition. The boxplots show the maximum, minimum, upper and lower quartiles, and the sample median. From left to right: n=13, n=18 and n=10 groups of 10-20 embryos.

hand2-positive LPM. In accordance with this hypothesis, LPM ventral migration was severely yet specifically impaired after SB431542 treatment and *ltbp3* knockdown (KD) at 48 hpf (Fig. 3C), whereas the total number of LPM/*hand2*+ cells did not change significantly in *Tg(hand2:EGFP)*^{pd24} embryos upon TGFβ inhibition (Fig. 3D and Fig. S3E). These data support a new role for TGFβ signaling in LPM-to-iSMC differentiation by promoting initial LPM migration.

To elucidate the downstream targets of TGFβ that might drive LPM migration and differentiation in iSMC, we analyzed transcriptomic data to identify: (1) genes induced by TGFβ – specifically and differentially expressed between human alveolar basal epithelial cells (A549) after 72 h of TGFβ induction and untreated cells (Sartor et al., 2010); (2) genes expressed in intestinal mesenchyme – specifically and differentially expressed between the mesenchymal and epithelial fraction of mouse intestine (Li et al., 2007) (Fig. S3F). Among those resulting genes, we focused our attention on *zeb1a* (zinc finger E-Box binding homeobox 1) and *foxo1a* (forkhead box protein O1), two transcription factor-encoding genes whose roles during the development of the GI tract remain unknown.

Zeb1a is required for LMP mesenchymalization and for iSMC differentiation

Zeb1a is a potent mediator of cell migration and invasion of tissues downstream of TGFβ signaling (Lamouille et al., 2014; Zhang et al., 2014). Accordingly, a specific role for Zeb1a during vascular SMC differentiation has been well established (Nishimura et al., 2006). However, a potential role for ZEB family members in iSMC development has not yet been determined. Therefore, we investigated whether ZEB1 is required for iSMC formation in zebrafish development using our two reporter transgenic lines. We silenced *zeb1a* in *Tg(acta2:mCherry)*^{uto5} and *Tg(hand2:EGFP)*^{pd24} embryos; injections of two independent *zeb1a* morpholinos (translation and splicing blocking) both abrogated iSMC development without affecting gut or endoderm development and morphology (Fig. 4A,B and Fig. S4A-C). To understand whether this defect was due to impaired LPM migration, we analyzed LPM morphology 48 hpf after silencing *zeb1a*. In *zeb1a*-impaired embryos, the LPM does not complete its migration and fails to cover the ventral region of the gut endoderm (Fig. 4C). We did not observe any significant differences in *hand2* expression levels compared with controls (Fig. S4D) nor in LPM/

Development (2017) 144, 464-478 doi:10.1242/dev.133926

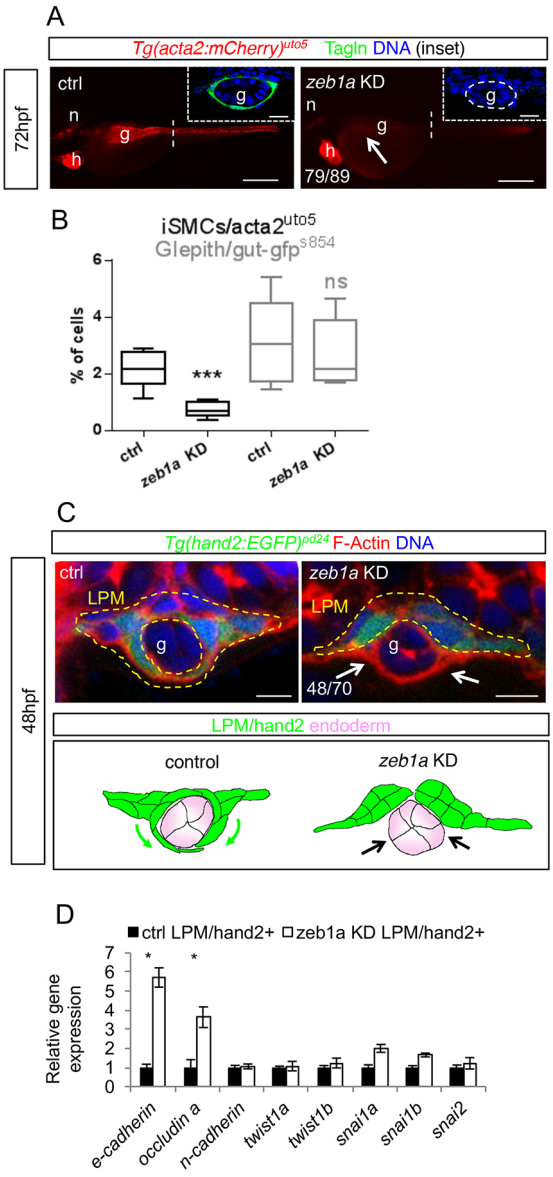

Fig. 4. TGFβ-driven LPM morphogenesis requires *zeb1a*. (A) Knockdown of the transcription factor *zeb1a* impairs iSMC differentiation. Fluorescent images of *Tg(acta2:mCherry)*^{uto5} embryos at 72 hpf after *zeb1a* morpholino injections. *zeb1a* knockdown embryos exhibit decreased mCherry and TagIn expression in the gut region (g) compared with controls (arrow). Scale bars: 200 µm. Insets show confocal transverse sections of the posterior gut region (dashed line) in embryos stained for TagIn (green). The number of embryos exhibiting the phenotype is indicated. Nuclei are in blue. Scale bars in insets: 10 µm. n, notochord; h, heart. (B) Knockdown of *zeb1a* does not alter endoderm morphology and differentiation. Box and whisker plots show the percentage of iSMCs or endodermal cells isolated by fluorescent-activated cell sorting (FACS) experiments from the trunk of double *Tg(acta2:mCherry)*^{uto5} *(Xia.Eef1a1:GFP)*^{s854} embryos at 72 hpf after *zeb1a* downregulation. Although the number of iSMCs is severely reduced by *zeb1a* knockdown, endodermal cells are normal. The boxplots show the maximum, minimum, upper and lower quartiles, and the sample median. Asterisks represent the results of unpaired *t*-tests of mean difference=0 (***P<0.001; n=6 groups of 10-20 embryos). (C) Knockdown of *zeb1a* impairs LPM ventral migration. Upper panel: confocal transverse sections of *Tg(hand2:EGFP)*^{pd24} stained with phalloidin (red). The number of embryos exhibiting this phenotype is indicated. Scale bars: 15 µm. Lower panel: schematic representation of impaired migration in *zeb1a* knockdown embryos. (D) *zeb1a* differentially regulates expression of genes associated with migrating phenotypes in LPM. Histograms show qPCR analyses of defined genes in LPM cells sorted from *Tg(hand2:EGFP)*^{pd24} after *zeb1a* knockdown and the relative controls at 48 hpf. Compared with controls, the knockdown of *zeb1a* upregulates genes (such as E-cadherin and occludin A) associated with non-migrating epithelial structures (*P<0.05).

hand2+ cell number (Fig. S4E). We also collected *hand2*+ cells from *zeb1a* knockdown embryos by FACS and analyzed a set of genes associated with mesenchymal migration by qPCR. Compared with controls, silencing of *zeb1a* markedly increased the expression of epithelial markers, including *cdh1* (E-cadherin) and *oclna* (occludin A), in the *hand2*-positive cell population. Such molecular features resemble the retention of the compact tight epithelial structure, possibly explaining the migration defects observed before (Fig. 4D).

Altogether, these data support a specific role for TGFβ signaling and *zeb1a* in driving LPM migration around the gut, a key step towards iSMC commitment. Once lateral-to-medial *hand2*-positive LPM migration has occurred, mesenchymal cells that now surround the endoderm start to differentiate into iSMCs.

Foxo1a is required for LPM and iSMC differentiation

Among the potentially TGFβ-regulated target genes in the intestinal mesenchyme and expressed in the LPM, we also identified *foxo1a*. Foxo1 belongs to the Forkhead family of transcription factors and regulates myogenic growth and differentiation, maintenance of stemness, and metabolism (Eijkelenboom and Burgering, 2013; Sanchez et al., 2014). A role for *foxo1a* in iSMC development has not been described previously. To investigate at which step of LPM-to-iSMC differentiation *foxo1a* might act, we knocked down *foxo1a* in *Tg(acta2:mCherry)*^{uto5} embryos with both a translational and splice-blocking morpholinos. In addition, we used AS1842856, a specific chemical inhibitor of Foxo1 activity (Nagashima et al., 2010) (Fig. S5A,B). Although *foxo1a* knockdown did not affect overall embryonic development (nor overall body morphology and gut endoderm morphology or differentiation), it impaired iSMC cell number and marker expression (Fig. S5A,C,D). We then evaluated whether *foxo1a* was required in the LPM. We found that both genetic and pharmacological inhibition of *foxo1a* reduced LPM/*hand2*+ cell number (Fig. 5A,B and Fig. S5E) and LPM proliferation (Fig. 5C). Nonetheless, *foxo1a* knockdown did not alter LPM migration (Fig. 5A) or the expression of genes associated with EMT and migration compared with controls (Fig. S5F). These data indicate that, complementary to our findings on *zeb1a* function, *foxo1a* is dispensable for LPM migration but it is required for LPM proliferation and maintenance.

To further understand the role of *foxo1a* in the LPM-to-iSMC differentiation, we performed *foxo1a* overexpression analysis and looked at the LPM differentiation state by measuring *hand2* expression levels as an indicator of the LPM versus iSMC differentiation state. Overexpression of *foxo1a* stimulated *hand2* expression in the embryo (Fig. 5D,E), impaired SMC marker expression and iSMC differentiation (Fig. 5D,F), and affected LPM cell number or proliferation (Fig. 5D and data not shown). These data propose *foxo1a* as a potent previously unrecognized molecular regulator of LPM during early zebrafish iSMC development. Altogether, our data reveal that Zeb1a and Foxo1a each control distinct roles in differentiating *hand2*-positive LPM (migration versus cell number/proliferation) towards forming functional iSMCs.

Development (2017) 144, 464-478 doi:10.1242/dev.133926

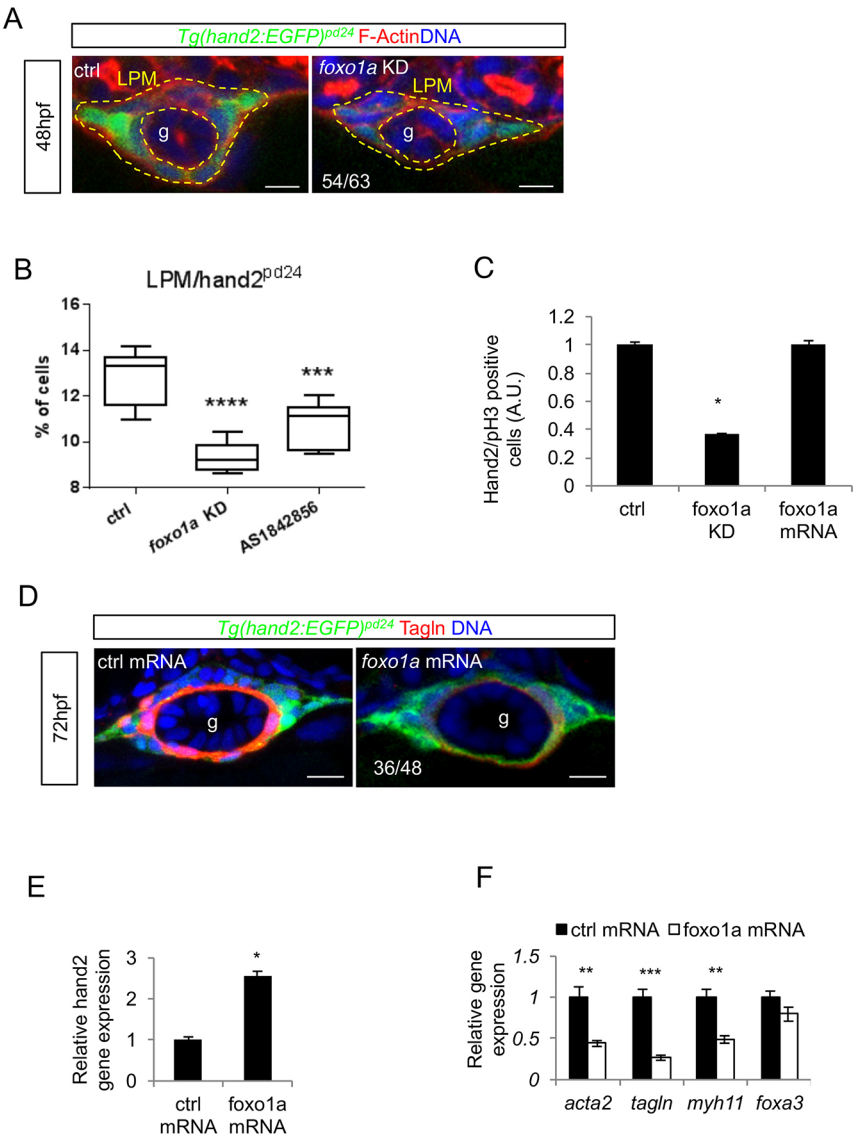

Fig. 5. Foxo1a is required for LPM commitment to iSMC differentiation. (A) *foxo1a* knockdown reduces the number of LPM cells without affecting migration. Confocal transverse sections of the gut (g) in *Tg(hand2:EGFP)*^{pd24} embryos injected with *foxo1a* morpholino and stained for phalloidin (red) at 48 hpf. The number of embryos showing fewer LPM cells is indicated. Nuclei are in blue. Scale bars: 15 µm. (B) Pharmacological and genetic *foxo1a* inhibition affect LPM. Box and whisker plots show the percentage of LPM cells isolated by fluorescent-activated cell sorting (FACS) experiments from trunks of *Tg(hand2:EGFP)*^{pd24} embryos 48 hpf after chemical (AS1842856) or genetic (*foxo1a* knockdown) *foxo1a* blockage. The boxplots show the maximum, minimum, upper and lower quartiles, and the sample median. Asterisks represent the results of one-way ANOVA-Dunnett's post-hoc test (***P<0.001, ****P<0.001; from left to right: n=12, n=6 and n=9 groups of 10-20 embryos). (C) *foxo1a* knockdown impaired LPM proliferation. The histogram shows the normalized count of pH3-positive cells in the LPM of *Tg(hand2:EGFP)*^{pd24} embryos at 48 hpf after *foxo1a* knockdown or overexpression (*P<0.05). (D) *foxo1a* mRNA overexpression blocks iSMC differentiation. Confocal transverse sections of *Tg(hand2:EGFP)*^{pd24} embryos at 72 hpf overexpressing *foxo1a* mRNA and stained for Tagln (red). The number of embryos exhibiting the phenotype is indicated. Nuclei are in blue. Scale bars: 15 µm. (E) *foxo1a* mRNA overexpression increases *hand2* expression. Histograms show *hand2* mRNA levels measured by qRT-PCR in *foxo1a*-overexpressing embryos compared with controls at 48 hpf (*P<0.05). (F) *foxo1a* mRNA overexpression affect iSMC marker expression. Histograms show *acta2*, *tagln*, *myh11* and *foxa3* mRNA levels measured by qRT-PCR in *foxo1a*-overexpressing embryos compared with controls at 72 hpf. The expression of endodermal marker *foxa3* is not altered (**P<0.01, ***P<0.001).

zeb1a and *foxo1a* are both regulated by the smooth muscle-specific *miR-145*

We next addressed the spatial and temporal expression of *zeb1a* and *foxo1a* in zebrafish, in particular if they are selectively expressed in LPM. We performed whole-mount *in situ* hybridization for *zeb1a* and *foxo1a* mRNA from 24 to 48 hpf stages (Fig. S6A,B). *zeb1a* is expressed mainly in a region surrounding the gut, possibly mesenchymal tissue. *foxo1a* expression is evident as early as 24 hpf in a bilateral region similar to the LPM stripes and in the gut region. Later on, *foxo1a* is also expressed in the endoderm as demonstrated by qPCR on endodermal *TgBAC(cldn15la-GFP)*^{pd1034}-sorted cells (Alvers et al., 2014; data not shown).

We next sought to explain the loss-of-function as well as gain-of-function phenotypes of these genes in LPM and iSMCs differentiation. We addressed how the complementary functions of *zeb1a* and *foxo1a* are temporally regulated and tuned, and whether a microRNA-based mechanism could be involved. *miR-145* is one of the most enriched microRNAs in SMCs where it contributes to the acquisition of the SMC fate and contractile state (Albinsson and Swärd, 2013; Boettger et al., 2009; Cordes et al., 2009; Elia et al., 2009; Xin et al., 2009). Previous work has found that *miR-145* expression is also regulated by TGFβ in vascular SMCs *in vitro* (Long and Miano, 2011). Therefore, we analyzed the expression of *miR-145* in developing zebrafish embryos and observed that its expression begins at the onset of iSMC maturation (~72 hpf) (Fig. 6A). *miR-145* was also strongly upregulated in *Tg(hsp70:caALK5)* embryos after heat shock, whereas chemical or genetic blockade of TGFβ signaling reduced *miR-145* expression (Fig. 6B,C). These data indicate that *mir-145* is also regulated by TGFβ signaling in iSMCs *in vivo* and are consistent with a conserved role for TGFβ signaling in *miR-145* regulation in both vascular and visceral SMCs (Long and Miano, 2011).

In zebrafish, *miR-145* seems highly and selectively expressed in intestinal SMCs (Wienholds et al., 2005; Zeng and Childs, 2012). Previous studies have shown that alterations in *miR-145* expression affect overall intestinal maturation (Zeng et al., 2009). To study the role of *miR-145* in iSMCs in more detail, we injected low doses of a *miR-145* dicer-blocking morpholino, sufficient to significantly reduce mature *miR-145* levels without altering endoderm differentiation and overall embryo morphology (Fig. S7A-C). Such *miR-145* KD embryos displayed fewer iSMCs in uneven

Development (2017) 144, 464-478 doi:10.1242/dev.133926

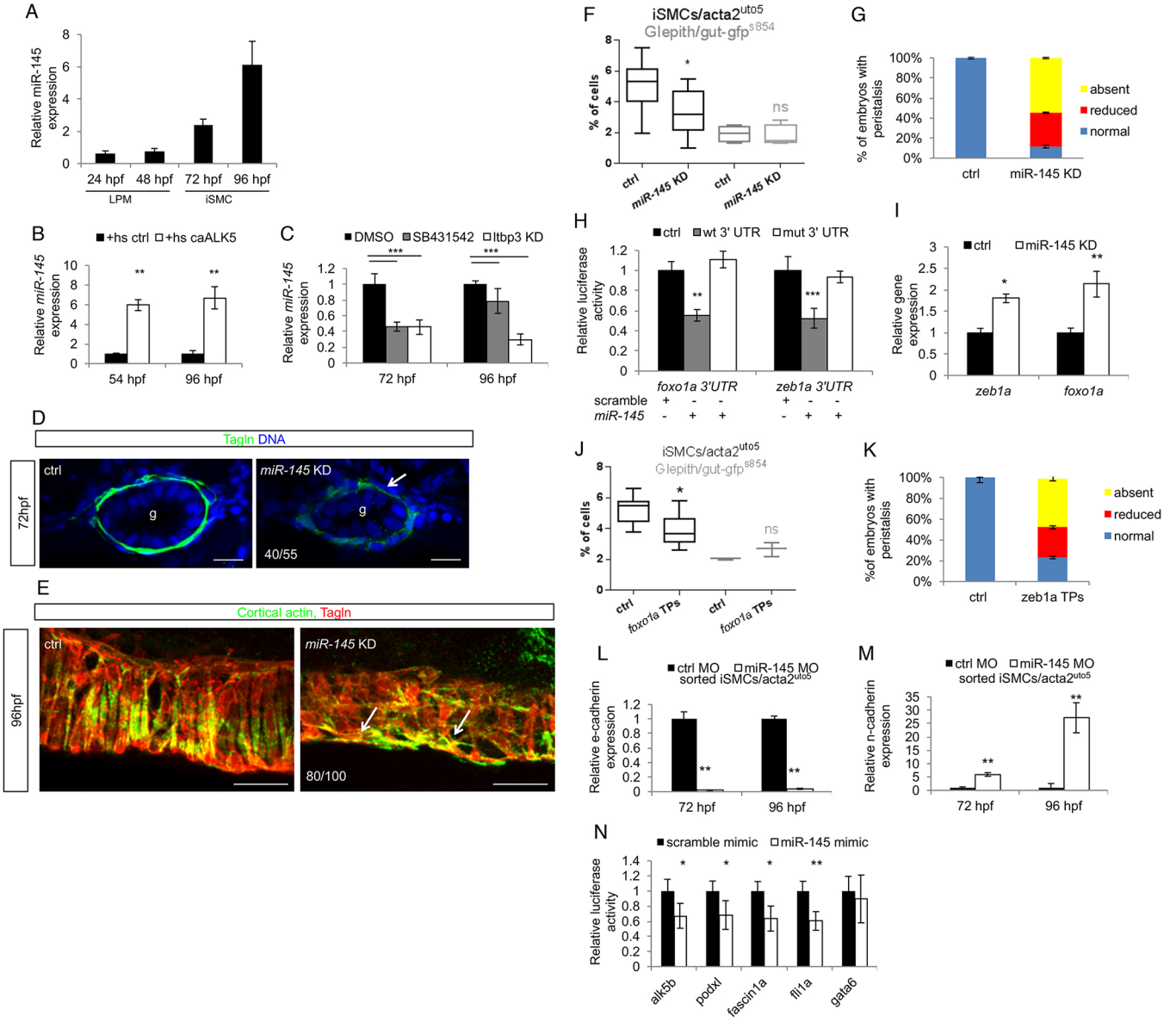

Fig. 6. See next page for legend.

layers around the gut (Fig. 6D). These embryos exhibited only a slight reduction in iSMC marker expression (Fig. S7D) and iSMC number (Fig. 5F). iSMCs in *miR-145*-impaired embryos showed an altered morphology that was typical of undifferentiated and synthetic SMCs being less stretched and more rounded compared with controls (Fig. 6E) (McHugh, 1996). Crucially, *miR-145* knockdown embryos showed severe contractility defects in iSMCs, including deficiencies in swim bladder inflation and gut peristalsis (Fig. S7C and Fig. 6G).

Since miRNAs function by binding and degrading target mRNAs (Bartel, 2009) and by regulating their translation, we sought to identify which protein-coding genes are targets of *miR-145* during iSMCs development. We filtered our list of 487 genes induced by TGFβ and expressed in the embryonic intestinal mesenchyme (Fig. S3F) for the presence of a *miR-145* binding site. We obtained a list of 41 putative *miR-145* targets conserved in human and mouse, containing several genes that had previously been confirmed to be *miR-145* targets (Table S3). Among them we found *foxo1a*, also predicted to be a target in zebrafish. Another gene was *zeb2*, which has recently been shown to be a direct target of *miR-145* (Ren et al., 2014). Within the ZEB gene family in zebrafish, *zeb1a* has a predicted *miR-145* target site. Combined, our data reveal that our identified iSMC regulators *foxo1a* and *zeb1a* are potential targets of the SMC-controlling microRNA *miR-145*.

To test whether *zeb1a* and *foxo1a* transcripts are physiologically relevant targets of *miR-145* during zebrafish SMC differentiation, we used complementary approaches. We first probed the ability of zebrafish *miR-145* to directly bind *zeb1a* and *foxo1a* 3′ UTR by luciferase experiments. To achieve this, we cloned the 3′ UTR of both genes into a luciferase reporter vector and performed reporter assays in HEK-293 cells expressing a zebrafish *miR-145* mimic or a scramble mimic as negative control. Luciferase expression from the reporter with the wild-type 3′ UTR of *zeb1a* was significantly repressed but was rescued after mutation of *miR-145* binding sites (Fig. 6H and Fig. S7E). We obtained analogous results with the 3′ UTR of the *foxo1a* gene (Fig. 6H and Fig. S7E). Next, given the

Development (2017) 144, 464-478 doi:10.1242/dev.133926

Fig. 6. Zeb1a and Foxo1a are regulated by the TGFβ-dependent miR-145 expression. (A) *miR-145* expression occurs from 72 hpf onwards in zebrafish embryos. Time-course analysis of *miR-145* expression in whole zebrafish embryos. qPCR was performed on total RNA extracted from embryos at the indicated developmental stages. Values are normalized to *miR-145* levels in unfertilized eggs. (B) Alk5 activation promotes *miR-145* transcription and maturation. Histograms show the levels of mature *miR-145* after activation of Alk5 signaling using the inducible *Tg(hsp70:caALK5)* line, as assessed by qRT-PCR analyses. (C) Blockade of Alk5 signaling significantly reduced mature *miR-145* levels. Histograms show the levels of mature *miR-145* after pharmacological (SB431542) and genetic (*ltbp3* knockdown) inactivation of Alk5 signaling compared with controls, as assessed by qRT-PCR. (D) *miR-145* knockdown in zebrafish embryos impairs iSMC maturation. Confocal transverse sections of *miR-145* knockdown embryos stained for Tagln (green). Knockdown of *miR-145* alters iSMC maturation as displayed by irregular morphology and shape of iSMCs compared with controls (arrow). The number of embryos exhibiting this phenotype is indicated. Nuclei are in blue. Scale bars: 15 µm. (E) *miR-145* knockdown alters iSMC organization in the intestine. Confocal maximum projection of iSMCs covering the gut after staining for Tagln (green) and cortical actin (red). *miR-145* knockdown embryos showed abnormal endoderm coverage and iSMC morphology (arrows) compared with controls. The number of embryos exhibiting this phenotype is indicated. Scale bars: 25 µm. (F) *miR-145* knockdown reduces iSMC number without affecting endoderm differentiation. Box and whisker plots show the percentage of iSMCs and endodermal cells isolated by fluorescent-activated cell sorting (FACS) experiments from the trunks of double *Tg(acta2:mcherry)*^{uto5} *(Xia.Eef1a1:GFP)*^{s854} embryos at 96 hpf after *miR-145* knockdown. The boxplots show the maximum, minimum, upper and lower quartiles, and the sample median. Asterisks represent the results of unpaired *t*-tests of mean difference=0 (**P*<0.05; from left to right: *n*=10, *n*=10, *n*=5 and *n*=5 groups of 10-20 embryos). (G) Loss of *miR-145* impairs gut peristalsis in zebrafish embryos. Histograms show the percentage of embryos with peristaltic gut movement at 96 hpf after *miR-145* knockdown. (H) Zebrafish *zeb1a* and *foxo1a* mRNA are directly bound by *miR-145*. The histogram shows luciferase activity in mammalian cells co-transfected with reporter constructs containing wild-type or mutant (mut) *zeb1a* and *foxo1a* 3′ UTR, together with a *miR-145* mimic or a scramble mimic. The results are shown as the mean±s.d. of Firefly luciferase activity relative to the controls, normalized with respect to Renilla luciferase activity. Asterisks represent the results of one-way ANOVA-Dunnett's post-hoc test (***P*<0.01, ****P*<0.001). (I) *miR-145* knockdown increases *foxo1a* and *zeb1a* levels as evaluated by qPCR on the trunk region of embryos at 96 hpf (**P*<0.05, ***P*<0.01). (J) The block of *miR-145* and *foxo1a* binding *in vivo* reduces iSMC number without affecting endoderm differentiation. Box and whisker plots show the percentage of iSMCs or endodermal cells isolated by fluorescent-activated cell sorting (FACS) experiments from the trunk of the double *Tg(acta2:mCherry)*^{uto5} *(Xia.Eef1a1:GFP)*^{s854} embryos at 96 hpf after *foxo1a* target protector (TPs) injection. The boxplots show the maximum, minimum, upper and lower quartiles, and the sample median. Asterisks represent the results of unpaired *t*-tests of mean difference=0 (**P*<0.05; from left to right: *n*=7, *n*=7, *n*=3 and *n*=3 groups of 10-20 embryos). (K) Block of *miR-145-zeb1a* binding *in vivo* affects gut peristalsis in zebrafish embryos. Histograms show the percentage of embryos with peristaltic gut movement at 96 hpf after *zeb1a* TP injections. (L,M) *miR-145* knockdown upregulates the mesenchymal program in iSMCs. Histograms show E-cadherin (L) and N-cadherin (M) mRNA levels evaluated by qRT-PCR in iSMCs sorted from *Tg(acta2:mCherry)*^{uto5} embryos after *miR-145* knockdown compared with control levels at 72 and 96 hpf. *miR-145* knockdown severely reduced E-cadherin mRNA levels but promoted N-cadherin mRNA expression. These data suggest that *miR-145* is required to switch off the mesenchymalization program in iSMCs responsible for their appearance (***P*<0.01). (N) *miR-145* directly targets Alk5 and several genes required for pEMT. Histograms show relative luciferase activity in cells co-transfected with reporter constructs containing the 3′ UTR of *alk5*, *podxl*, *fascin1a*, *fli1a* and *gata6* together with a *miR-145* mimic or a scramble mimic. The results are shown as the mean±s.d. of Firefly luciferase activity relative to controls, normalized to Renilla luciferase activity. The data indicate that *miR-145* targets the Alk5 receptor, as well as other mesenchymal genes, such as *podxl*, *fascin* and *fli1a* (**P*<0.05, ***P*<0.01). *gata6*, a known *miR-145* target, was used as a control.

unavailability of antibodies to measure Zeb1a and Foxo1a protein levels, we measured the relative abundance of endogenous *zeb1a* and *foxo1a* transcripts in control and experimentally manipulated embryos by quantitative PCR (Fig. 6I). Injection of *miR-145* morpholino resulted in a ∼2-fold increase in *zeb1a* and *foxo1a* expression levels. These data demonstrate that endogenous *zeb1a* and *foxo1a* transcript levels change in response to decreased *miR-145* activity. Finally, to address the consequence of *miR-145*-dependent downregulation of *zeb1a* or *foxo1a* during iSMC differentiation, we specifically blocked the *miR-145*-mediated downregulation of *zeb1a* and *foxo1a* in live embryos using target protector technology (Staton, 2011). Injections of *zeb1a* or *foxo1a* target protectors (*zeb1a-TP* or *foxo1a*-TP) in zebrafish embryos specifically impaired iSMC differentiation. *foxo1a-TP* injection reduced the number of iSMCs (Fig. 6J) whereas *zeb1a-TP* injection affected iSMC contractility (Fig. 6K). Strikingly, co-injection of *foxo1a*-TP and *zeb1a*-TP phenocopied *miR-145* knockdown embryos, including fewer *hand2*-positive iSMCs with disorganized layer architecture (Fig. S7F), indicating that *miR-145*-mediated targeting of *zeb1a* and *foxo1a* mRNA are both required to complete iSMC differentiation and maturation.

We hypothesized that *miR-145* is required for differentiation of iSMCs after migration and to allow immature iSMCs to become peristaltic/mature iSMCs. We measured the mesenchymal state of iSMCs in *miR-145* knockdown embryos by analyzing the ratio of *cdh1* versus *cdh2* (N-cadherin) expression. iSMCs with *miR-145* knockdown exhibited severe downregulation of *cdh1* and, concomitantly, significant upregulation of *cdh2* (Fig. 6L,M). Using luciferase assays, we next determined that *miR-145* negatively regulated other target genes known to mediate migration, including *podxl*, *fscn1a* (fascin actin-bundling protein 1A) and *fli1a* (Feng et al., 2014; Larsson et al., 2009; Lin et al., 2014) (Fig. 5N). Interestingly, we found that *alk5b* was also a bona fide target of *miR-145* (Fig. 6N), suggesting the existence of a negative-feedback loop between *miR-145* and the TGFβ pathway that is responsible for *miR-145* induction.

Altogether, these data suggest that *miR-145* is required for iSMC maturation and for the acquisition of contractile properties downstream of initial iSMC fate commitment and LPM mesenchymalization and migration. In addition, our results propose that TGFβ-*zeb1a* and *foxo1a* regulate LPM morphogenesis and the initial step of LPM-to-iSMC differentiation. The *miR-145* expression driven by TGFβ signaling is then required in immature *hand2*-positive iSMCs to: (1) switch off the mesenchymal program governed by Foxo1a and the migration programs controlled by Zeb1a; and (2) to promote maturation of iSMCs into contractile and fully differentiated SMCs.

DISCUSSION

Despite their biological and clinical importance, the origin and differentiation of gastrointestinal SMC have been scarcely investigated to date, in particular compared with studies of vascular SMC or endoderm development. Here, using the zebrafish model system, we have studied the developmental origin of vertebrate iSMCs and have identified a genetic program responsible for iSMC differentiation and maturation.

Our data provide evidence that identifies the LPM as the lineage that gives rise to SMCs in the GI tract of zebrafish embryos by combining reporter transgene imaging and genetic lineage-tracing experiments using the LPM-expressed *drl:creERT2* (Mosimann et al., 2015). Our lineage-tracing results provide the first genetic confirmation in vertebrate that smooth muscle cells in the gut region are derived from lateral mesodermal organ precursors. These findings are consistent with and extend previous cell culture and transplantation experiments performed in *Xenopus* and chick,

Development (2017) 144, 464-478 doi:10.1242/dev.133926

respectively, that provided the first indications that the LPM gives rise to iSMCs (Chalmers and Slack, 2000; Roberts et al., 1998). iSMC formation happens notably later than the medial migration and differentiation of other LPM-derived lineages, including the bilateral precursors for cardiovascular, hematopoietic and renal cell fates that functionally remodel prior to 24 hpf in zebrafish. The absence of obvious defects in the other LPM-derived lineages after TGFβ/*zeb1a* and *foxo1a* modulations suggests that these genes are active only in the iSMC-fated LPM population, or that compensatory mechanisms exist in other lineages. Curiously, the sole posterior phenotype of *hand2* mutations in zebrafish is the lack of iSMCs, suggesting a dedicated role for *hand2* in the posterior LPM stripe that is fated to form intestinal smooth muscle.

We identified TGFβ as a crucial regulator of LPM-to-iSMC differentiation that sustains LPM ventral migration around the endoderm. The TGFβ superfamily consists of several different protein families, including TGFβ proteins, bone morphogenetic proteins (BMPs), activins, Nodal and many others. Our data suggest that a key role in LPM-to-iSMC differentiation is played by the TGFβ type I receptor Alk5, which is targeted by both the inhibitors we used in this study (SB431542 and LY364947). In addition, previous work has also shown that *ltbp3* inhibition phenocopies the effect of LY364947 treatments in zebrafish hearts (Zhou et al., 2011). Furthermore, chemical inhibition of BMP signaling does not affect iSMCs in zebrafish (Table S2), indicating once again a specific role for TGFβ proteins. However, more-detailed genetic studies are needed to understand the precise receptors and ligands involved in this process and to exclude the involvement of other signaling molecules.

Despite being a mesodermal tissue, LPM has been described as a polarized epithelium (before 30 hpf) by expression and apical localization of aPKC (Horne-Badovinac et al., 2003). We now show that markers of mesenchymalization (e.g. N-cadherin) are also already present at this developmental stages, questioning the nature of undifferentiated LPM as bona fide epithelium. Later on during development, LPM/*hand2*+ cells migrate around the gut to give rise to iSMC precursors (48 hpf) in a process that we found to be dependent on Alk5/TGFβ signaling. We reasoned that an important role for TGFβ/*zeb1a* could be to promote the acquisition of migratory phenotype for LPM. In particular, LPM migration could be driven by a TGFβ-induced partial EMT process. Indeed, unlike canonical EMT, which transforms epithelial layers into individual motile mesenchymal cells, LPM migrates as a cohesive layer of mesenchymal cells. The LPM thus retains at the same time epithelial features such as cell-cell contacts and a supracellular organization, and mesenchymal features such as migration and the ability of ECM remodeling (Yin et al., 2010).

Interestingly, we also found that the migration program in the differentiating LPM could be switched off by *miR-145*, a microRNA that has already been shown to modulate EMT acting as a tumor suppressor gene in other contexts. In particular, being able to directly bind the 3′ UTRs of *oct4* and *zeb2* transcripts, *miR-145* has been considered as a regulator of invasion and stem cell properties in prostate and lung cancer (Hu et al., 2014; Ren et al., 2014). Our data show that *miR-145* regulates iSMC development and differentiation in similar manner by regulating LPM migration and proliferation and homeostasis via *zeb1a* and *foxo1a* repression, respectively. *miR-145* expression is controlled by TGFβ as master regulator of migration, invasion and EMT, and that *miR-145* in turn represses several TGFβ downstream target genes. This interplay establishes an autoregulatory negative-feedback loop that spatiotemporally demarcates LPM migration. Other work showed that *miR-145* regulates, and is regulated by, TGFβ signaling in other cell types (Long and Miano, 2011; Zhao et al., 2015), reinforcing the existence of such a feedback loop. Nonetheless, we noticed that *miR-145* expression occurs later than initial TGFβ activation, suggesting the existence of a regulatory mechanism that keeps *miR-145* transcriptionally silent until its action is needed. More-detailed insights are required into the genetic and epigenetic mechanisms of *miR-145* transcriptional regulation in the smooth muscle field and cancer. Besides its role in cancer progression, *miR-145* has been found as one of the most enriched miRNAs in vascular smooth muscle cells (vSMCs), where *miR-145* is required for vSMC maturation and further regulation of their plasticity and contractility (Albinsson and Swärd, 2013; Boettger et al., 2009; Chivukula et al., 2014; Cordes et al., 2009; Elia et al., 2009; Xin et al., 2009). Many *miR-145* target genes have been shown to be involved in these processes; yet, our newly found connection to *zeb1a* and *foxo1a* in iSMCs also suggests that these two novel players might be involved in the regulation of smooth muscle cell plasticity.

By analyzing the direct targets of *miR-145*, we identified Foxo1a as a potent and unforeseen player in intestinal smooth muscle differentiation. Forkhead box O (FOXO) transcription factors are involved in widespread regulation of the cell cycle, apoptosis and metabolism (Eijkelenboom and Burgering, 2013). Support for a role for Foxo1 in smooth muscle cell differentiation also arises from work on mesodermal precursor cells derived from mouse *Foxo1*$^{-/-}$ embryonic stem cells (ESCs) that fail to form vascular smooth muscle cells (Park et al., 2009). *In vitro* ESC differentiation models revealed that Foxo1 activity plays a key role in progenitor cell and stem cell maintenance: Foxo1 is an essential component of the cellular control mechanism that maintains pluripotency in human embryonic stem cells (hESCs) through direct control of *OCT4* and *SOX2* gene expression by occupation and activation of their respective promoters (Zhang et al., 2011). In the same model system, Xu and co-workers have reported that expression of *miR-145* is low in self-renewing hESCs but highly upregulated during differentiation via direct binding and repression of *OCT4*, *SOX2* and *KLF4* (Xu et al., 2009). Here, we demonstrate that *foxo1a* expression is enriched in the *hand2*+ zebrafish LPM and its absence impairs LPM patterning and differentiation. Furthermore, our data reveal that *foxo1a* overexpression maintains the undifferentiated/embryonic state of LPM as *hand2*-positive tissue. We propose a model where *miR-145* expression is required to drive mesoderm lineage-restricted differentiation into SMCs by repressing expression of Foxo1. A role for *foxo1a* in endoderm-derived tissues is conceivable during development, although this function must be unrelated to its regulation by miRNA-145. Overall, we report here that Foxo1 is a direct target of *miR-145*, which in turn supports the previously unforeseen link between *miR145* and stemness via Foxo1.

In summary, we have genetically established that the iSMCs are a cell fate of the LPM, and we have uncovered a new molecular pathway that promotes the coordinated cellular events that drive the LPM towards iSMC differentiation during vertebrate development (Fig. 7). In particular, we have found that *miR-145*, *zeb1a* and *foxo1a* are interconnected key players during iSMC differentiation in zebrafish. Our findings propose a new regulatory pathway through which TGFβ/Alk5 input commits the *hand2*-positive LPM stripes towards forming iSMC precursors by tuning a tissue-specific mesenchymalization process via *zeb1a* and *miR-145* expression. In particular, *miR-145* provides Alk5 signaling with a broadly acting tool to influence the downstream post-transcriptional dynamics of

Development (2017) 144, 464-478 doi:10.1242/dev.133926

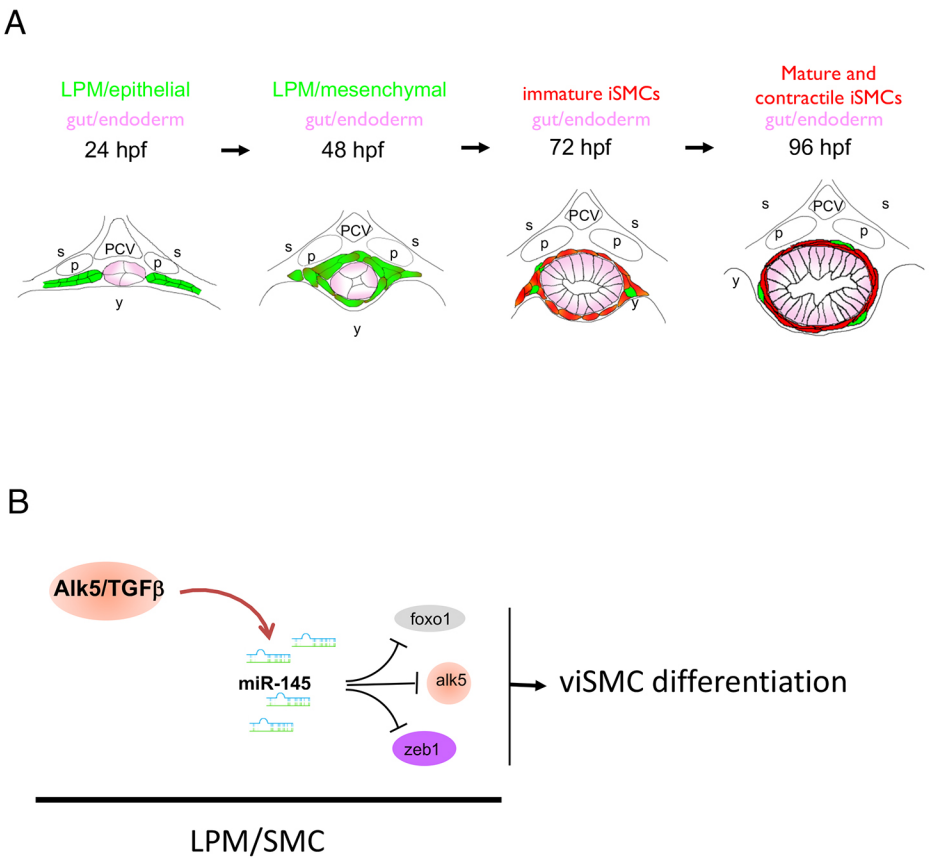

Fig. 7. Schematic model of the molecular and cellular events of iSMC development and differentiation in zebrafish. (A) By 24 hpf, the remaining undifferentiated LPM (green) has migrated towards the endodermal rod (pink) at the midline. By 48 hpf, the LPM has migrated around the endoderm, which involves TGFβ/Zeb1a signaling. *foxo1a* was also required in the LPM to promote LPM differentiation. By 72 hpf, the LPM cells began to express early smooth muscle markers, such as Tagln and Acta2, and became immature iSMCs. p, pronephros; PCV, posterior cardinal vein; s, somite; y, yolk. (B) During iSMC commitment, *miR-145* expression was activated by TGFβ signaling. *miR-145* was required to switch off the Zeb1a-mediated mesenchymalization genetic program and generate a negative-feedback loop of TGFβ signaling. *miR-145* was also required to downregulate *foxo1a*, stop the proliferation and allow differentiation of iSMCs.

mesenchymalization. In parallel, we have identified *foxo1a* as an LPM-expressed gene involved in iSMC differentiation that is also regulated by the Alk5 and *miR-145* signaling. Alteration in these developmental processes can result in genetic disorders, such as visceral myopathy. Our work provides a new molecular framework from which to analyze these molecular players for their prognostic and therapeutic potential in human gastrointestinal genetic diseases and cancers arising from dedifferentiated iSMCs (Spoelstra et al., 2006; Wangler et al., 2014; Yamamoto and Oda, 2015).

MATERIALS AND METHODS

Zebrafish lines

Zebrafish were handled according to established protocols and maintained under standard laboratory conditions. The *Tg(hsp70l:Hsa.TGFBR1_T204D-HA,cryaa:Cerulean)*^{fb6Tg} [referred to as *Tg(hsp70:caALK5)*], *TgBAC(hand2:EGFP)*^{pd24}, *Tg(Xla.Eef1a1:GFP)*^{s854}, *TgBAC(cldn15la-GFP)*^{pd1034}, *Tg(-6.4drl:creERT2)* and *ubi:Switch* lines have been described previously (Mosimann et al., 2015; Mosimann and Zon, 2011; Ober et al., 2006; Rohr et al., 2006; Yin et al., 2010; Zhou et al., 2011; Alvers et al., 2014). The generation of the *Tg(acta2:mCherry)*^{uto5} and *Tg(tagln:EGFP)*^{uto37} lines is described below. Following fertilization, embryos were collected and grown in the presence of 0.003% 1-phenyl-2-thiourea (PTU, Sigma-Aldrich) to prevent the formation of melanin pigment.

Promoter analyses and generation of the zebrafish transgenic lines

We analyzed the list of transcription factors represented by JASPAR positional weight matrices (Table S1). For *acta2*, the AVID alignment tool from VISTA has been used to directly align the region spanning from 2 kb upstream of the TSS to the end of the first intron of ACTA2 in zebrafish, human and mouse. We located the predicted binding sites in the *D. rerio* genome for the above-mentioned transcription factors using a log-likelihood ratio score, with the background nucleotide frequencies computed over the entire intergenic fraction of the *D. rerio* genome. The cutoff score was set to 66% of the best possible score for the PWM or an absolute score greater than 9. The Tol2-based *acta2:mCherry* and *tagln:EGFP-CAAX* constructs were assembled using the Tol2 Kit and a three-fragment gateway recombination cloning strategy (Kwan et al., 2007). For 5′ entry cloning, ∼350 bp of the *acta2* promoter was amplified from the genomic DNA of wild-type zebrafish by PCR with the following primers containing appropriate *attB4* and *attB1r* sites: 5′-GGGGACAACTTTGTATAGAAAAGTTGGCCATTCCTTCTCAGGTGTGG-3′ and 5′-GGGGACTGCTTTTTTGTACAAACTTGGGCACTTACCCTGACAGTGC-3′, respectively. The PCR product was then cloned into *pDONRP4-P1R* by BP reaction to obtain *p5E-acta2*. For middle entry cloning, the zebrafish *acta2* first intron was amplified with the following primers containing appropriate attB1 and attB2 sites: 5′-GGGGACAAGTTTGTACAAAAAAGCAGGCTACCTAGCTTCTCTCACCTCC-3′ and 5′-GGGGACCACTTTGTACAAGAAAGCTGGGTTTTCAGCTCGGATATCCTTTCTTACTCC-3′, respectively, and cloned into *pDONR221* by BP reaction. The 3′ entry clone was *p3E-mCherrypA*. Entry vectors were assembled in the *pDestTol2pA2* vector by LR reaction to create the *pDestTol2-acta2-mCherry-pA* vector. For the *tagln* gene, ClustalW alignment was used to align the region spanning 2 kb upstream of the TSS of *tagln* in four different fish species (zebrafish, Tetraodon, stickleback and medaka). This multiple alignment was used as input to calculate the log-likelihood ratio score of the transcription factor binding represented by JASPAR positional weight matrices. The score cutoff was set to 50% of the best possible score for the PWM. For generation of the *tagln:CAAX-EGFP* construct, the 2 kb *tagln* promoter was amplified from the genomic DNA of wild-type zebrafish with the following primers containing appropriate *attB4* and *attB1* sites: 5′-GGGGACAACTTTGTATAGAAAAGTTGAGACGACAGAATAGAGAGGGCGGTGT-3′ and 5′-GGGGACTGCTTTTTTGTACAAACTTGCAGCAGCTTTATGTTCAGCACGG-3′, respectively. The PCR product was then cloned into *pDONRP4-P1R* by BP reaction to obtain p5E-*tagln*. *pME-EGFP-CAAX* was used as a middle element, and the 3′ element was *p3E-polyA*. Entry vectors were assembled with the vector

Development (2017) 144, 464-478 doi:10.1242/dev.133926

pDestTol2pA2 by LR reaction to create the vector pDestTol2-tagln-EGFPCAAX-pA. The vectors were mixed with mRNA for *Tol2* transposase and microinjected into one-cell stage wild-type embryos. Injected embryos were raised to adulthood, and founders were screened for red fluorescence in SMCs. The transgenic fish line names *Tg(acta2:mCherry)*^{uto5} and *Tg(tagln:CAAX-EGFP)*^{uto37} were approved by the Zebrafish Nomenclature Committee of the ZFIN (http://zfin.org).

Immunofluorescence staining

Immunofluorescence was performed as previously described (Santoro et al., 2009). Briefly, embryos were fixed in 4% paraformaldehyde at 4°C overnight and washed three times in PBS. For immunofluorescence on sections, embryos were embedded in 4% low-melting agarose (Sigma-Aldrich). Sections (250 µm) were obtained using a vibratome (VT1000 S, Leica), permeabilized with 1% BSA, 1% DMSO and 0.3% Triton X-100 in PBS for 30 min at room temperature, and then incubated with primary antibody at 4°C overnight. After washing in PBS-T (0.1% Triton X-100 and 1% BSA in PBS), the sections were incubated with secondary antibodies (Alexa Fluor, Life Technologies) and Hoechst 33342 (Life Technologies) for 4 h at room temperature. The sections were washed in PBS-T, followed by PBS, then mounted on slides with Vectashield (Vector Labs). For whole-mount immunofluorescence, the fixed embryos were permeabilized in 1% DMSO and 1% Triton X-100 for 30 min at room temperature and then blocked in 4% BSA and 0.3% Triton X-100 in PBS for 4 h at room temperature. Embryos were incubated with the primary antibody at 4°C overnight, washed and incubated with secondary antibodies for 2 h at room temperature. After the washes, the embryos were embedded in 4% low-melting agarose and sectioned at the vibratome. The sections were mounted on slides with Vectashield. A polyclonal anti-transgelin antibody was produced using the C-terminal sequence (Santoro et al., 2009). For neuronal staining, the monoclonal antibody anti-Hu was used (1:50; mAB 16A11, Molecular Probes). For LPM staining, antibody anti-N-cadherin (1:200, Genetex) and aPKC (1:200, SantaCruz) were used. For actin staining, the sections were permeabilized and incubated with fluorescein isothiocyanate-labeled (1:1000 for 2 h at room temperature; Sigma-Aldrich) or tetramethylrhodamine B isothiocyanate-labeled (1:500 for 2 h at room temperature; Sigma-Aldrich) phalloidin after the washes.

Confocal and stereo microscopy analyses

Images were acquired with a TCSII SP5X confocal microscope, a MZ16 FA stereomicroscope equipped with a DCF300FY camera (Leica) or a AZ100 stereomicroscope equipped with an AxioCam MRm camera (Zeiss). The LAS AF and Zen software suites were used for analysis and image processing. Whole-embryo confocal images were acquired using the tile scan and automated mosaic merge functions of Leica LAS AF software. Digital micrograph images were contrast balanced, color matched, cropped and rotated using Photoshop 7 (Adobe).

Genetic lineage-tracing experiments

Cell-tracing experiments were performed essentially as previously described (Felker et al., 2016; Mosimann and Zon, 2011). Briefly, embryos from *Tg(-6.4drl:creERT2)* (Mosimann et al., 2015) and *ubi:Switch* line intercross were treated with fresh 10 µM 4-OH tamoxifen (H7904, Sigma-Aldrich) in DMSO at the one-somite stage, with subsequent thorough washing of the embryos in untreated E3 medium at 24 hpf. At the indicated time points, embryos were fixed and processed for confocal analyses.

Whole-mount *in situ* hybridization

The *in situ* hybridization probes were designed with an oligonucleotide-based method. An oligonucleotide pair (including T7 promoter) was used to amplify target region (CDS or 3′UTR) from zebrafish cDNA, followed by *in vitro* transcription including DIG-labeled NTPs (Roche). Afterwards, RNA was precipitated with lithium chloride, washed with 75% ethanol and dissolved in DEPC water. RNA quality was checked on a MOPS gel. For the *zeb1a in situ* hybridization probe, the following primers were used: GAG-GAGTGCGTCAGTGATGAGG and TAATACGACTCACTATAGGCA-GGTGCTCCTTCAGGTGATGC (rev with T7). For the *foxo1a in situ* hybridization probe the following primers were used: GTGGAGCTAAA-TTGCAAGGACG and TAATACGACTCACTATAGGCGTGTAAACTC-TCTGTACACCG (rev with T7).

Flow-activated cell sorter experiments

Embryos were disaggregated into single cells as previously described (Mugoni et al., 2013). A FACSCalibur flow cytometer (BD Biosciences) and the Cell Quest software were used to measure the percentage of fluorescent cells. A FACS ARIA III sorter (BD Biosciences) was used to isolate single cells for subsequent RNA extraction.

Chemical treatments on zebrafish embryos

Chemicals for zebrafish treatments were dissolved in DMSO. Zebrafish embryos were treated with the following drugs: SB431548 (50 µM; Sigma-Aldrich); AS1842856 (100 nM; Calbiochem); LY364947 (50 µM; Sigma-Aldrich); purmorphamine (10-100 µM; Calbiochem); cyclopamine (50 µM; Calbiochem); dorsomorphin (10-100 µM; Sigma-Aldrich); LDN193189 (250 nM-1 µM; Sigma-Aldrich); GM6001 (50-200 µM; Merck Millipore); SU1498 (5-100 µM; Calbiochem); SU5416 (10-100 µM; Sigma-Aldrich); L-NAME (100-500 µM; Sigma-Aldrich); SNAP (100-500 µM; Sigma-Aldrich); and PDGFR tyrosine kinase inhibitor V 521234 (1-100 µM; Calbiochem). The treatments were administered from 20 to 72 hpf. Chemicals were refreshed daily.

Gene knockdown experiments

Gene knockdown experiments were performed by microinjecting morpholinos (Table S4) into zebrafish embryos at the one-cell stage. Morpholinos were synthetized from GeneTools and dissolved in nuclease-free water. The primers for testing the efficacy of the *zeb1a* morpholino were designed using the zebrafish *zeb1a* sequence (GenBank accession number: XM_001344071.6) and are as follows: *zeb1a*_ex2_Fw, 5′-GCGACCTC-AGATTCAGATG-3′; *zeb1a*_ex3_Rv, 5′-TGACCCTTATTTCTCGTATT-AAAG-3′; and *zeb1a*_in2_Rv, 5′-CTATGTGATTGTGCCTGATG-3′. The primers for testing knockdown by the *foxo1a* morpholino were designed for zebrafish *foxo1a* (GenBank accession number NM_001077257.2) and are as follows: *foxo1a*_ex2_Fw, 5′-GGGAAAAGTGGAAAGTCTCC-3′; *foxo1a*_ex3_Rv, 5′-TGTGTGGGTGAGAAAGAGTG-3′; and *foxo1a*_in2 _Rv, 5′-TGAATGTGGCCTGAATGAG-3′. As a control, β-actin was detected with the following primers: *β-actin*_Fw, 5′-GTATCCACGAGACCACCTTCA-3′; and *β-actin*_Rv, 5′-GAGGAGGGCAAAGTGGTAAAC-3′.

Heat shock experiments

Heat-shock experiments on *Tg(hsp70l:Hsa.TGFBR1_T204D-HA,cryaa:Cerulean)*^{fb6Tg} were performed essentially as previously described (Zhou et al., 2011) by administering a 37°C heat shock for 1 h to transgenic and clutch mate controls. For *miR-145* analyses, embryos were heat shocked at 48 hpf and 72 hpf, and RNA from the trunk was extracted after 6 and 24 h, respectively. For coding gene analyses, embryos were heat shocked at 48 hpf and RNA from trunk was extracted after 24 h.

Analysis of mammalian gene expression profiling

Data from a previous study (Sartor et al., 2010) were analyzed to obtain a list of genes differentially expressed between A459 cells after 72 h of TGFβ induction and untreated cells. Using limma (Smyth, 2005) and a false discovery rate (FDR) of 0.01, 1725 upregulated probes and 1444 downregulated probes corresponding to 1010 and 981 unique genes, respectively, were obtained. Similarly, data from Li et al. (2007) were analyzed to obtain a list of genes differentially expressed between the mesenchymal and epithelial fractions of mouse intestine. Using limma and an FDR cutoff of 0.01, we found that 9272 probes were upregulated in the mesenchymal fraction and 3595 were downregulated, corresponding to 5380 and 2384 unique genes, respectively.

miR-145 target analysis

The *miR-145* target predictions were based on the latest TargetScan release (6.2). In particular, we used the mouse orthologs of the human annotations for mouse predictions and the annotated zebrafish UTRs for zebrafish

Development (2017) 144, 464-478 doi:10.1242/dev.133926

predictions (Ulitsky et al., 2012). Gene overlaps and comparisons between different species were based on the Homologene (build66) orthology database.

Peristalsis analysis on zebrafish embryos

Embryos were anesthetized with 0.04 mg/ml tricaine (Sigma-Aldrich), mounted in 3% methyl cellulose (Sigma-Aldrich), and allowed to adapt for 5 min before recording. Each embryo was recorded for 1 min with an MZ16 FA stereomicroscope equipped with a DCF300FY camera (Leica). The frequency and amplitude of peristaltic movements were compared between controls and injected embryos. Forty embryos per group were analyzed in two independent experiments.

Luciferase assay experiments

Luciferase reporter vectors containing the 3′ UTR of the indicated *miR-145* target genes were generated by PCR amplification of the 3′ UTR from zebrafish genomic DNA and subsequent cloning into the Firefly luciferase reporter pMIR-REPORT vector (Ambion). When indicated, the 3′ UTRs were mutagenized or deleted at the *miR-145* recognition site using the QuikChange Site-Directed Mutagenesis kit (Stratagene), according to the manufacturer's instructions with the primers listed below. A total of 5×10^4 HEK293 cells was co-transfected with 50 ng of the pMIR-REPORT (Ambion) Firefly luciferase constructs containing the 3′ UTRs of the indicated *miR-145* potential target genes and 20 ng of pRL-TK Renilla luciferase normalization control (Promega) using Lipofectamine 2000 (Invitrogen Life Technologies). Lysates were collected 48 h after transfection, and Firefly and Renilla luciferase activities were measured with a Dual-Luciferase Reporter System (Promega). The *foxo1a* 3′ UTR was amplified with the following primers: *foxo1a_3′UTR*_Fw, 5′-GTGGAGCTAAATTGCAAGGAC-3′; and *foxo1a_3′UTR*_Rv, 5′-TTAACCACGCCCCTCTTATG-3′. *miR-145* binding sites were mutated in *foxo1a* 3′ UTR using the following primers: *foxo1a*_Mut1_Fw, 5′-GGGAAGAAGCCCGGGTGAGCGGGAATCGCTG-3′; *foxo1a*_Mut1_Rv, 5′-CAGCGATTCCCGCTCACCCGGGCTTCTTCCC-3′; *foxo1a*_Mut2_Fw, 5′-GTAAATCGGAGAGATCCCGGGTTCGACGTTTTTAC-3′; and *foxo1a*_Mut2_Rv, 5′-GTAAAAACGTCGAACCCGGGATCTCTCCGATTTAC-3′.

The *zeb1a* 3′ UTR was amplified with the following primers: *zeb1a_3′UTR*_Fw, 5′-CTTACAGGGGTGATTCTCATG-3′; and *zeb1a_3′UTR*_Rv, 5′-AACGACTGACACGTTACACAC-3′. *miR-145* binding sites were deleted in the *zeb1a* 3′ UTR using the following primers: *zeb1a*_Mut1_Fw, 5′-CAAATTTATGCGTATTCCCGGGTGCTGCACGATATTGG-3′; *zeb1a*_Mut1_Rv, 5′-CCAATATCGTGCAGCACCCGGGAATACGCATAAATTTG-3′; *zeb1a*_Mut2_Fw, 5′-CTTTTCACAATCTTCAGTGTTTGTCATTTGATCCCGGGAGAGTTTCTCACGTGTTGTTTGATT-3′; and *zeb1a*_Mut2_Rv, 5′-AATCAAACAACACGTGAGAAACTCTCCCGGGATCAAATGACAAACACTGAAGATTGTGAAAAG-3′.

Quantitative real-time PCR analyses

RNA was isolated with TRIzol reagent (Invitrogen Life Technologies), and cDNA was made with a RT High Capacity kit (Applied Biosystems), according to the manufacturer's protocol. qRT-PCR was performed with an ABI 7900HT Fast Real-Time PCR System (Applied Biosystems) using Platinum qPCR SuperMix-UDG with ROX (Invitrogen Life Technologies). The following genes were analyzed: *acta2* (NM_212620.1); *tagln* (NM_001045467.1); *myh11* (NM_001024448.1); *foxa3* (NM_131299.1); *foxo1a* (NM_001077257.2); *zeb1a* (XM_001344071.6); *hand2* (NM_131626.2); E-cadherin (NM_131820.1); N-cadherin (NM_131081.2); occludin A (NM_212832.2); *twist1a* (NM_130984.2); *twist1b* (NM_001017820.1); *snai1a* (NM_131066.1); *snai1b* (NM_130989.3); and *snai2* (NM_001008581.1). The β-actin gene (*actb*) was included as a control housekeeping gene (NM_131031.1 and NM_181601.4). Specific primers were designed with the dedicated UPL on-line tool (Roche) and are provided in Table S5. Data were analyzed using the ΔΔCt method with ABI software, version 2.1 (Applied Biosystems). For microRNA analyses, RNA was extracted using the TRIzol reagent (Invitrogen Life Technologies). qRT-PCR for microRNA detection was performed with the indicated TaqMan microRNA assays (Applied Biosystems) on 10 ng of total RNA according to the manufacturer's instructions. qRT-PCR was conducted using gene-specific primers on a 7900HT Fast Real-Time PCR System (Applied Biosystems). Quantitative normalization was performed for the expression of the RNU6 small nucleolar RNA. Data analysis was performed using the ΔΔCt method with the ABI software, version 2.1 (Applied Biosystems).

Northern blot analyses

Total RNA (20 µg) isolated as above was resolved by 12.5% (w/v) TBE-urea-polyacrylamide gel electrophoresis and transferred to a Hybond N+ membrane (GE Healthcare Life Sciences). The filter was hybridized overnight at 45°C with a specific *miR-145* digoxigenin-labeled LNA detection probe (Exiqon), washed and visualized with a specific DIG antibody (1:10,000) using the DIG Nucleic Acid Detection kit (all from Roche). The filter was then stripped and re-probed overnight at 45°C using a specific U6 digoxigenin-labeled LNA detection probe (Exiqon).

hand2-positive cell proliferation analyses

Phosphohistone H3 (Ser10, Cell Signaling) immunofluorescence was used to evaluate cell proliferation. The staining was performed on cross-sections of the gut of *Tg(hand2:EGFP)*^{pd24} at 48 hpf. Ph3/*hand2* double-positive cells and *hand2* single-positive cells were counted in a minimum of three distinct sections per embryo in eight individual animals. The ratios are represented normalized to controls.

foxo1a overexpression experiments

The complete zebrafish *foxo1a* CDS was amplified by PCR from cDNA using the primers: *foxo1a*_Fw, 5′-GTACCATGGCTGACGCAG-3′ and *foxo1a*_Rv, 5′-CTACCCAGACACCCAGCTG-3′. Purified PCR product was cloned in *pCS2+* vector. *foxo1a* mRNA was synthesized using the mMessage Machine kit (Ambion) following the manufacturer's instructions. Wild-type embryos were injected at the one-cell stage with 100 pg of *foxo1a* mRNA. We also included a control mRNA encoding the fluorescent protein mCherry (100 pg) in each injection.

Statistical analyses

All experiments were performed at least three independent times for each condition, and the error bars represent the mean±s.d. of the mean unless otherwise stated. Statistical significance was evaluated by Student's test or one-way ANOVA-Dunnett's post-hoc test as appropriate, and significance is reported as $*P<0.05$, $**P<0.01$, $***P<0.001$ and $****P<0.0001$.

Acknowledgements

We thank Vanessa Barone for cloning the *acta2* promoter and generating the *Tg(acta2:mCherry)*^{uto5} line, Dr Caroline E. Burns for providing the *Tg(hsp70:caALK5)* line, Dr M. Bagnat for providing *Tg(claudin:GFP)* line, Anastasia Felker for assistance with genetic lineage tracing, Xiaowen Chen for assistance with rescue experiments and members of the Santoro lab for critical reading of the manuscript.

Competing interests

The authors declare no competing or financial interests.

Author contributions

D.G. and M.M.S. planned and discussed the entire project. U.A. and P.P. performed the bioinformatic analyses of gene expression, *miR-145* targets, and *acta2* and *tagln* promoters. A.C. assisted with the FACS analyses. C.M. and C.H. provided transgenic *Tg(drl:CreERT2)* lines, performed cell lineage and whole-mount *in situ* hybridization experiments, and contributed to data interpretation. M.M.S. and D.G. wrote the manuscript.

Funding

This work was supported by a Human Frontier Science Program Career Developmental Award, by Marie Skłodowska-Curie actions (IRG 247852), by Fondazione Telethon (GGP10185), and Horizon 2020 grant ERC-CoG-647057 (all awarded to M.M.S.). Funding was also received from the Canton of Zürich, from a Swiss National Science Foundation professorship (PP00P3_139093) and from a Marie Skłodowska-Curie actions Career Integration Grant to C.M. C.H. was supported by Universität Zürich Forschungskredit.

Supplementary information

Supplementary information available online at
http://dev.biologists.org/lookup/doi/10.1242/dev.133926.supplemental

Development (2017) 144, 464-478 doi:10.1242/dev.133926

References

Albinsson, S. and Swärd, K. (2013). Targeting smooth muscle microRNAs for therapeutic benefit in vascular disease. *Pharmacol. Res.* **75**, 28-36.

Alvers, A. L., Ryan, S., Scherz, P. J., Huisken, J. and Bagnat, M. (2014). Single continuous lumen formation in the zebrafish gut is mediated by smoothened-dependent tissue remodeling. *Development* **141**, 1110-1119.

Bagnat, M., Cheung, I. D., Mostov, K. E. and Stainier, D. Y. (2007). Genetic control of single lumen formation in the zebrafish gut. *Nat. Cell Biol.* **9**, 954-960.

Bartel, D. P. (2009). MicroRNAs: target recognition and regulatory functions. *Cell* **136**, 215-233.

Boettger, T., Beetz, N., Kostin, S., Schneider, J., Krüger, M., Hein, L. and Braun, T. (2009). Acquisition of the contractile phenotype by murine arterial smooth muscle cells depends on the Mir143/145 gene cluster. *J. Clin. Invest.* **119**, 2634-2647.

Chalmers, A. D. and Slack, J. M. (2000). The Xenopus tadpole gut: fate maps and morphogenetic movements. *Development* **127**, 381-392.

Chivukula, R. R., Shi, G., Acharya, A., Mills, E. W., Zeitels, L. R., Anandam, J. L., Abdelnaby, A. A., Balch, G. C., Mansour, J. C., Yopp, A. C. et al. (2014). An essential mesenchymal function for miR-143/145 in intestinal epithelial regeneration. *Cell* **157**, 1104-1116.

Cordes, K. R., Sheehy, N. T., White, M. P., Berry, E. C., Morton, S. U., Muth, A. N., Lee, T. H., Miano, J. M., Ivey, K. N. and Srivastava, D. (2009). miR-145 and miR-143 regulate smooth muscle cell fate and plasticity. *Nature* **460**, 705-710.

Davidson, A. J. and Zon, L. I. (2004). The 'definitive' (and 'primitive') guide to zebrafish hematopoiesis. *Oncogene* **23**, 7233-7246.

Eijkelenboom, A. and Burgering, B. M. T. (2013). FOXOs: signalling integrators for homeostasis maintenance. *Nat. Rev. Mol. Cell Biol.* **14**, 83-97.

Elia, L., Quintavalle, M., Zhang, J., Contu, R., Cossu, L., Latronico, M. V. G., Peterson, K. L., Indolfi, C., Catalucci, D., Chen, J. et al. (2009). The knockout of miR-143 and -145 alters smooth muscle cell maintenance and vascular homeostasis in mice: correlates with human disease. *Cell Death Differ.* **16**, 1590-1598.

Felker, A., Nieuwenhuize, S., Dolbois, A., Blazkova, K., Hess, C., Low, L. W. L., Burger, S., Samson, N., Carney, T. J., Bartunek, P. et al. (2016). In vivo performance and properties of tamoxifen metabolites for CreERT2 control. *PLoS ONE* **11**, e0152989.

Feng, Y., Zhu, J., Ou, C., Deng, Z., Chen, M., Huang, W. and Li, L. (2014). MicroRNA-145 inhibits tumour growth and metastasis in colorectal cancer by targeting fascin-1. *Br. J. Cancer* **110**, 2300-2309.

Gabella, G. (2002). Development of visceral smooth muscle. *Results Probl. Cell Differ.* **38**, 1-37.

Georgijevic, S., Subramanian, Y., Rollins, E.-L., Starovic-Subota, O., Tang, A. C. Y. and Childs, S. J. (2007). Spatiotemporal expression of smooth muscle markers in developing zebrafish gut. *Dev. Dyn.* **236**, 1623-1632.

Gering, M., Yamada, Y., Rabbitts, T. H. and Patient, R. K. (2003). Lmo2 and Scl/Tal1 convert non-axial mesoderm into haemangioblasts which differentiate into endothelial cells in the absence of Gata1. *Development* **130**, 6187-6199.

Horne-Badovinac, S., Rebagliati, M. and Stainier, D. Y. (2003). A cellular framework for gut-looping morphogenesis in zebrafish. *Science* **302**, 662-665.

Hu, J., Qiu, M., Jiang, F., Zhang, S., Yang, X., Wang, J., Xu, L. and Yin, R. (2014). MiR-145 regulates cancer stem-like properties and epithelial-to-mesenchymal transition in lung adenocarcinoma-initiating cells. *Tumour Biol.* **35**, 8953-8961.

Kloosterman, W. P. and Plasterk, R. H. A. (2006). The diverse functions of microRNAs in animal development and disease. *Dev. Cell* **11**, 441-450.

Kumar, M. S. and Owens, G. K. (2003). Combinatorial control of smooth muscle-specific gene expression. *Arterioscler. Thromb. Vasc. Biol.* **23**, 737-747.

Kwan, K. M., Fujimoto, E., Grabher, C., Mangum, B. D., Hardy, M. E., Campbell, D. S., Parant, J. M., Yost, H. J., Kanki, J. P. and Chien, C.-B. (2007). The Tol2kit: a multisite gateway-based construction kit for Tol2 transposon transgenesis constructs. *Dev. Dyn.* **236**, 3088-3099.

Lamouille, S., Xu, J. and Derynck, R. (2014). Molecular mechanisms of epithelial–mesenchymal transition. *Nat. Rev. Mol. Cell Biol.* **15**, 178-196.

Larsson, E., Fredlund Fuchs, P., Heldin, J., Barkefors, I., Bondjers, C., Genové, G., Arrondel, C., Gerwins, P., Kurschat, C., Schermer, B. et al. (2009). Discovery of microvascular miRNAs using public gene expression data: miR-145 is expressed in pericytes and is a regulator of Fli1. *Genome Med.* **1**, 108.

Li, X., Madison, B. B., Zacharias, W., Kolterud, A., States, D. and Gumucio, D. L. (2007). Deconvoluting the intestine: molecular evidence for a major role of the mesenchyme in the modulation of signaling cross talk. *Physiol. Genomics* **29**, 290-301.

Lim, J. and Thiery, J. P. (2012). Epithelial-mesenchymal transitions: insights from development. *Development* **139**, 3471-3486.

Lin, C.-W., Sun, M.-S., Liao, M.-Y., Chung, C.-H., Chi, Y.-H., Chiou, L.-T., Yu, J., Lou, K.-L. and Wu, H.-C. (2014). Podocalyxin-like 1 promotes invadopodia formation and metastasis through activation of Rac1/Cdc42/cortactin signaling in breast cancer cells. *Carcinogenesis* **35**, 2425-2435.

Long, X. and Miano, J. M. (2011). Transforming growth factor-beta1 (TGF-beta1) utilizes distinct pathways for the transcriptional activation of microRNA 143/145 in human coronary artery smooth muscle cells. *J. Biol. Chem.* **286**, 30119-30129.

McHugh, K. M. (1996). Molecular analysis of gastrointestinal smooth muscle development. *J. Pediatr. Gastroenterol. Nutr.* **23**, 379-394.

Mosimann, C. and Zon, L. I. (2011). Advanced zebrafish transgenesis with Tol2 and application for Cre/lox recombination experiments. *Methods Cell Biol.* **104**, 173-194.

Mosimann, C., Panáková, D., Werdich, A. A., Musso, G., Burger, A., Lawson, K. L., Carr, L. A., Nevis, K. R., Sabeh, M. K., Zhou, Y. et al. (2015). Chamber identity programs drive early functional partitioning of the heart. *Nat. Commun.* **6**, 8146.

Mugoni, V., Postel, R., Catanzaro, V., De Luca, E., Turco, E., Digilio, G., Silengo, L., Murphy, M. P., Medana, C., Stainier, D. Y. et al. (2013). Ubiad1 is an antioxidant enzyme that regulates eNOS activity by CoQ10 synthesis. *Cell* **152**, 504-518.

Nagashima, T., Shigematsu, N., Maruki, R., Urano, Y., Tanaka, H., Shimaya, A., Shimokawa, T. and Shibasaki, M. (2010). Discovery of novel forkhead box O1 inhibitors for treating type 2 diabetes: improvement of fasting glycemia in diabetic db/db mice. *Mol. Pharmacol.* **78**, 961-970.

Nishimura, G., Manabe, I., Tsushima, K., Fujiu, K., Oishi, Y., Imai, Y., Maemura, K., Miyagishi, M., Higashi, Y., Kondoh, H. et al. (2006). DeltaEF1 mediates TGF-beta signaling in vascular smooth muscle cell differentiation. *Dev. Cell* **11**, 93-104.

Ober, E. A., Verkade, H., Field, H. A. and Stainier, D. Y. R. (2006). Mesodermal Wnt2b signalling positively regulates liver specification. *Nature* **442**, 688-691.

Olden, T., Akhtar, T., Beckman, S. A. and Wallace, K. N. (2008). Differentiation of the zebrafish enteric nervous system and intestinal smooth muscle. *Genesis* **46**, 484-498.

Park, S.-H., Sakamoto, H., Tsuji-Tamura, K., Furuyama, T. and Ogawa, M. (2009). Foxo1 is essential for in vitro vascular formation from embryonic stem cells. *Biochem. Biophys. Res. Commun.* **390**, 861-866.

Reichenbach, B., Delalande, J.-M., Kolmogorova, E., Prier, A., Nguyen, T., Smith, C. M., Holzschuh, J. and Shepherd, I. T. (2008). Endoderm-derived Sonic hedgehog and mesoderm Hand2 expression are required for enteric nervous system development in zebrafish. *Dev. Biol.* **318**, 52-64.

Ren, D., Wang, M., Guo, W., Huang, S., Wang, Z., Zhao, X., Du, H., Song, L. and Peng, X. (2014). Double-negative feedback loop between ZEB2 and miR-145 regulates epithelial-mesenchymal transition and stem cell properties in prostate cancer cells. *Cell Tissue Res.* **358**, 763-778.

Roberts, D. J., Smith, D. M., Goff, D. J. and Tabin, C. J. (1998). Epithelial-mesenchymal signaling during the regionalization of the chick gut. *Development* **125**, 2791-2801.

Rohr, S., Bit-Avragim, N. and Abdelilah-Seyfried, S. (2006). Heart and soul/PRKCi and nagie oko/Mpp5 regulate myocardial coherence and remodeling during cardiac morphogenesis. *Development* **133**, 107-115.

Rørth, P. (2012). Fellow travellers: emergent properties of collective cell migration. *EMBO Rep.* **13**, 984-991.

Sanchez, A. M. J., Candau, R. B. and Bernardi, H. (2014). FoxO transcription factors: their roles in the maintenance of skeletal muscle homeostasis. *Cell. Mol. Life Sci.* **71**, 1657-1671.

Santoro, M. M., Pesce, G. and Stainier, D. Y. (2009). Characterization of vascular mural cells during zebrafish development. *Mech. Dev.* **126**, 638-649.

Sartor, M. A., Mahavisno, V., Keshamouni, V. G., Cavalcoli, J., Wright, Z., Karnovsky, A., Kuick, R., Jagadish, H. V., Mirel, B., Weymouth, T. et al. (2010). ConceptGen: a gene set enrichment and gene set relation mapping tool. *Bioinformatics* **26**, 456-463.

Shyer, A. E., Tallinen, T., Nerurkar, N. L., Wei, Z., Gil, E. S., Kaplan, D. L., Tabin, C. J. and Mahadevan, L. (2013). Villification: how the gut gets its villi. *Science* **342**, 212-218.

Smyth, G. K (2005). Limma: linear models for microarray data. In *Bioinformatics and Computational Biology Solutions using R and Bioconductor* (R. Gentleman, V. Carey, S. Dudoit, R. Irizarry and W. Huber, eds), pp.397-420. New York: Springer.

Solway, J., Seltzer, J., Samaha, F. F., Kim, S., Alger, L. E., Niu, Q., Morrisey, E. E., Ip, H. S. and Parmacek, M. S. (1995). Structure and expression of a smooth muscle cell-specific gene, SM22 alpha. *J. Biol. Chem.* **270**, 13460-13469.

Spoelstra, N. S., Manning, N. G., Higashi, Y., Darling, D., Singh, M., Shroyer, K. R., Broaddus, R. R., Horwitz, K. B. and Richer, J. K. (2006). The transcription factor ZEB1 is aberrantly expressed in aggressive uterine cancers. *Cancer Res.* **66**, 3893-3902.

Stainier, D. Y. R. (2005). No organ left behind: tales of gut development and evolution. *Science* **307**, 1902-1904.

Staton, C. A. (2011). Class 3 semaphorins and their receptors in physiological and pathological angiogenesis. *Biochem. Soc. Trans.* **39**, 1565-1570.

Tsang, J., Zhu, J. and van Oudenaarden, A. (2007). MicroRNA-mediated feedback and feedforward loops are recurrent network motifs in mammals. *Mol. Cell* **26**, 753-767.

Ulitsky, I., Shkumatava, A., Jan, C. H., Subtelny, A. O., Koppstein, D., Bell, G. W., Sive, H. and Bartel, D. P. (2012). Extensive alternative polyadenylation during zebrafish development. *Genome Res.* **22**, 2054-2066.

Wallace, K. N., Akhter, S., Smith, E. M., Lorent, K. and Pack, M. (2005). Intestinal growth and differentiation in zebrafish. *Mech. Dev.* **122**, 157-173.

Development (2017) 144, 464-478 doi:10.1242/dev.133926

Wangler, M. F., Gonzaga-Jauregui, C., Gambin, T., Penney, S., Moss, T., Chopra, A., Probst, F. J., Xia, F., Yang, Y., Werlin, S. et al. (2014). Heterozygous de novo and inherited mutations in the smooth muscle actin (ACTG2) gene underlie megacystis-microcolon-intestinal hypoperistalsis syndrome. *PLoS Genet.* **10**, e1004258.

Whitesell, T. R., Kennedy, R. M., Carter, A. D., Rollins, E.-L., Georgijevic, S., Santoro, M. M. and Childs, S. J. (2014). An alpha-smooth muscle actin (acta2/alphasma) zebrafish transgenic line marking vascular mural cells and visceral smooth muscle cells. *PLoS ONE* **9**, e90590.

Wienholds, E., Kloosterman, W. P., Miska, E., Alvarez-Saavedra, E., Berezikov, E., de Bruijn, E., Horvitz, H. R., Kauppinen, S. and Plasterk, R. H. A. (2005). MicroRNA expression in zebrafish embryonic development. *Science* **309**, 310-311.

Xin, M., Small, E. M., Sutherland, L. B., Qi, X., McAnally, J., Plato, C. F., Richardson, J. A., Bassel-Duby, R. and Olson, E. N. (2009). MicroRNAs miR-143 and miR-145 modulate cytoskeletal dynamics and responsiveness of smooth muscle cells to injury. *Genes Dev.* **23**, 2166-2178.

Xu, N., Papagiannakopoulos, T., Pan, G. J., Thomson, J. A. and Kosik, K. S. (2009). MicroRNA-145 regulates OCT4, SOX2, and KLF4 and represses pluripotency in human embryonic stem cells. *Cell* **137**, 647-658.

Yamamoto, H. and Oda, Y. (2015). Gastrointestinal stromal tumor: recent advances in pathology and genetics. *Pathol. Int.* **65**, 9-18.

Yelon, D., Ticho, B., Halpern, M. E., Ruvinsky, I., Ho, R. K., Silver, L. M. and Stainier, D. Y. (2000). The bHLH transcription factor hand2 plays parallel roles in zebrafish heart and pectoral fin development. *Development* **127**, 2573-2582.

Yin, C., Kikuchi, K., Hochgreb, T., Poss, K. D. and Stainier, D. Y. R. (2010). Hand2 regulates extracellular matrix remodeling essential for gut-looping morphogenesis in zebrafish. *Dev. Cell* **18**, 973-984.

Zeng, L. and Childs, S. J. (2012). The smooth muscle microRNA miR-145 regulates gut epithelial development via a paracrine mechanism. *Dev. Biol.* **367**, 178-186.

Zeng, L., Carter, A. D. and Childs, S. J. (2009). miR-145 directs intestinal maturation in zebrafish. *Proc. Natl. Acad. Sci. USA* **106**, 17793-17798.

Zhang, X., Yalcin, S., Lee, D.-F., Yeh, T.-Y. J., Lee, S.-M., Su, J., Mungamuri, S. K., Rimmelé, P., Kennedy, M., Sellers, R. et al. (2011). FOXO1 is an essential regulator of pluripotency in human embryonic stem cells. *Nat. Cell Biol.* **13**, 1092-1099.

Zhang, J., Tian, X.-J., Zhang, H., Teng, Y., Li, R., Bai, F., Elankumaran, S. and Xing, J. (2014). TGF-beta-induced epithelial-to-mesenchymal transition proceeds through stepwise activation of multiple feedback loops. *Sci. Signal.* **7**, ra91.

Zhao, N., Koenig, S. N., Trask, A. J., Lin, C.-H., Hans, C. P., Garg, V. and Lilly, B. (2015). MicroRNA miR145 regulates TGFBR2 expression and matrix synthesis in vascular smooth muscle cells. *Circ. Res.* **116**, 23-34.

Zhou, Y., Cashman, T. J., Nevis, K. R., Obregon, P., Carney, S. A., Liu, Y., Gu, A., Mosimann, C., Sondalle, S., Peterson, R. E. et al. (2011). Latent TGF-beta binding protein 3 identifies a second heart field in zebrafish. *Nature* **474**, 645-648.